J_ID: ZA1 Customer A_ID: 07-0056.R1 Cadmus Art: JBMM32018 Date: 15-MARCH-08 Stage: I Page: 2

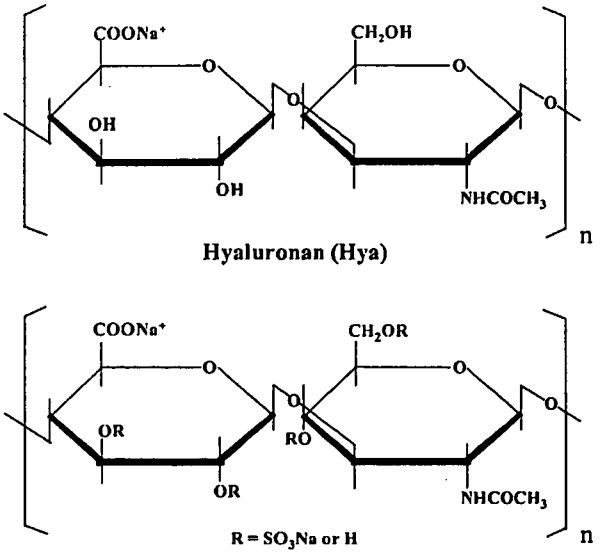

Figure 1. Structure of Hya and SHya. SHya is composed of Hya and a sulfate group. The molecular weight of SHya is 2.0×10^4, and the degree of substitution of SHya is 0.6.

MATERIALS AND METHODS

SHya preparation

SHya was synthesized by the method reported earlier (Fig. 1).[11] The molecular weight of SHya was 2.0×10^4, and the degree of substitution (D.S.) of SHya was 0.6, as determined by the chelate titration method.[12] Briefly, 2% Hya120 (molecular weight, 1.2×10^6) solution in *N,N*-dimethylformamide (DMF) (Wako Pure Chemical Industries, Osaka, Japan) was mixed with trimethylamine (TMA)-SO_3 complex (Aldrich Chemical, Milwaukee, WI) and stirred at 60°C for 24 h. The reaction mixture was then diluted, neutralized, and precipitated by adding acetone (Wako Pure Chemical Industries). The precipitate was dissolved in distilled water and dialyzed against distilled water. Moreover, the effectiveness of sulfation was also demonstrated by FTIR analysis. The IR spectrum of SHya exhibited two absorption bands at 1240 and 820 cm^{-1} due to S=O and SO_3^- stretching, respectively. Stock solutions of SHya were made directly in ABM medium (Cambrex Bio Science, Walkersville, MD) supplemented with 5% FCS, and recombinant human epidermal growth factor.

Astrocyte cell culture

NHA (Cambrex Bio Science) was maintained in ABM medium supplemented with 5% FCS, and recombinant human epidermal growth factor, and cultured in a humidified atmosphere of 5% CO_2 under 95% air at 37°C.

Giemsa staining

When the cells reached confluence in tissue culture dishes, cells were fixed and stained with Giemsa solution. Cell morphology was determined under an inverted light microscope.

MTT assay for cell proliferation

NHA was seeded into 24-well plates for MTT assay at a density of 1×10^4/well in ABM medium supplemented with 5% FCS, recombinant human epidermal growth factor, and cultured in a humidified atmosphere of 5% CO_2 under 95% air at 37°C. After 1-week culture with different concentrations of SHya (10 or 50 μg/mL), the viability of NHA cells was determined by MTT assay. TetraColor ONE (Seikagaku Kogyo, Tokyo, Japan) was used to measure changes in cell numbers. This assay measures the activity of the enzyme in mitochondria for counting living cells. The medium was replaced with 300 μL of fresh medium containing 6 μL TetraColor ONE reagents. After 2 h, samples were measured in a microplate reader.

Scrape loading and dye transfer assay

The scrape loading and dye transfer (SLDT) technique was performed by the method of El-Fouly et al.[13] Confluent monolayer cells in 35-mm culture dishes were rinsed with Ca^{2+}, Mg^{2+} phosphate-buffered saline [PBS(+)], and the cell dishes were loaded with 0.1% Lucifer Yellow (Molecular Probes, Eugene, OR) in PBS(+) solution and immediately scraped with a sharp blade. After incubation for 5 min at 37°C, cells were washed four times with PBS(+), and the extent of dye transfer was monitored using a fluorescence microscope equipped with a type UFX-DXII CCD camera and a super high-pressure mercury lamp power supply (Nikon, Tokyo, Japan).

Expression of gap junctional and neural cell marker genes

For quantitative RT-PCR, NHA was seeded into 12-well plates at a density of 2×10^4 cells/well in ABM medium (Cambrex Bio Science) supplemented with 5% FCS, and recombinant human epidermal growth factor, and cultured in a humidified atmosphere of 5% CO_2 under 95% air at 37°C. After 1-week cell culture with 10 or 50 μg/mL SHya, single-stranded cDNA was prepared from 1 μg of total RNA by reverse transcription (RT) using a commercially available First-Strand cDNA Kit (Amersham Pharmacia Biotech, Uppsala, Sweden). Aliquots of the cDNA (1/20) were used as templates for PCR analysis using a Lightcycler System (Roche, Mannheim, Germany). PCR amplification was performed in a total volume of 20 μL mixture including 1 μL of RT reaction mixture, 2 μL Light Cycler-Fast Start Reaction Mix SYBR Green 1 (Roche), 0.5 μ*M* each primer, and 3 m*M* $MgCl_2$. The PCR program consisted of 40 cycles of 8 s at 94°C, 5 s at 65°C, and 10 s at 72°C. Primer sequences for amplification were

ID: sangeethag Date: 15/3/08 Time: 13:51 Path: J:/Production/JBMM/VOL00000/080132/3B2/C2JBMM080132

J_ID: ZA1 Customer A_ID: 07-0056.R1 Cadmus Art: JBMM32018 Date: 15-MARCH-08 Stage: I Page: 3

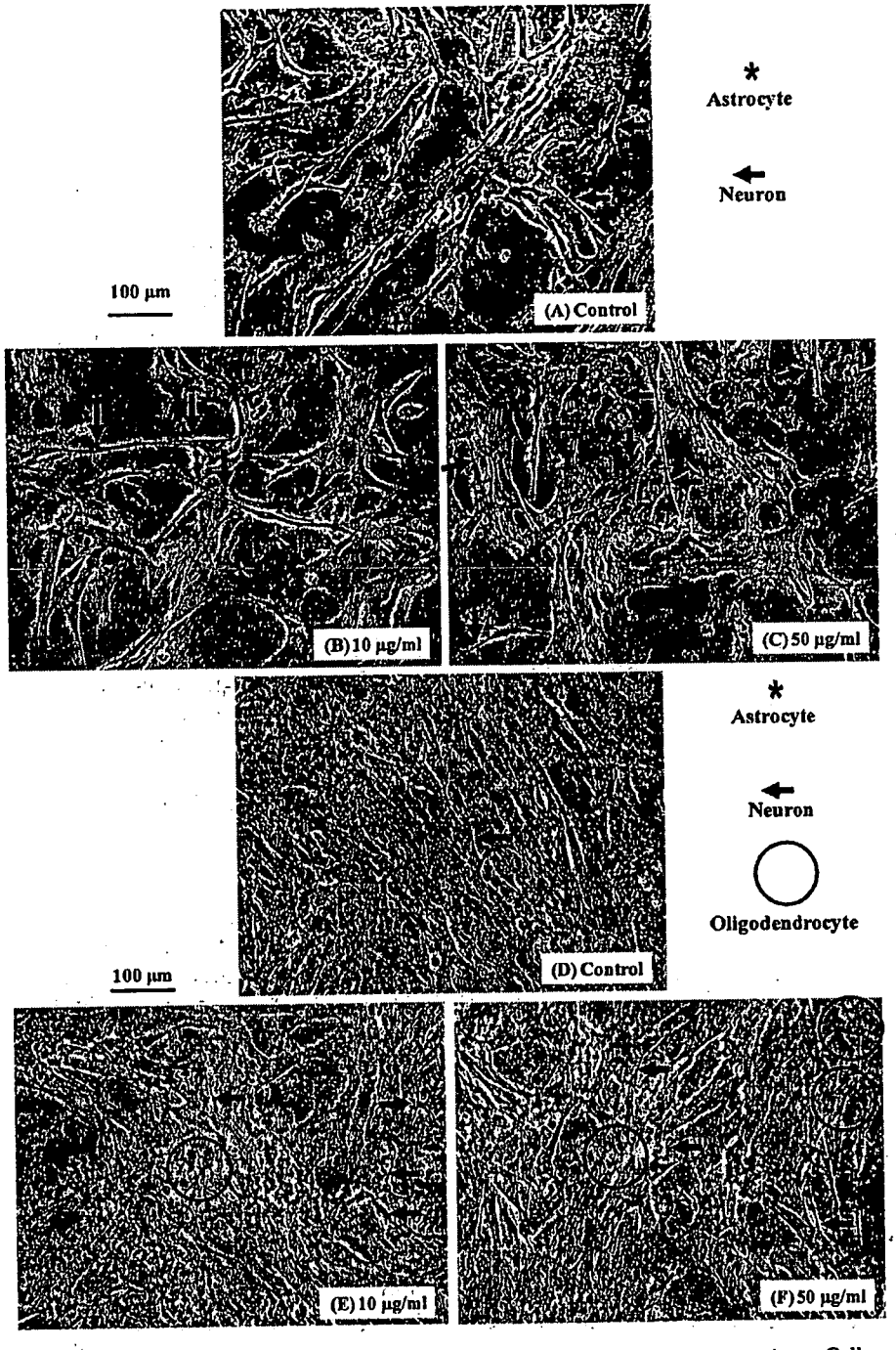

Figure 2. NHA cell morphology. Cultures were cultured with SHya in different concentrations. Cells were observed by inverted light microscopy observation and Giemsa staining. After 3 days of culture, some cells looked like the branches or spikes extending out from the cell body (neuron) in control (A) and 10 μg/mL (B) of SHya-treated cultures, and the neurons were elongated and increased in number in 50 μg/mL (C) of SHya-treated cultures. After 1 week, in addition to neuron, some cells appeared like the sparse branches of a tree (oligodendrocyte) with 10 μg/mL (E) and 50 μg/mL (F) of SHya. The number of oligodendrocytes was increased at 50 μg/mL of SHya-treated cultures, compared with the control (D) culture.

5′-GGGCTAATTACAGTGCAG-3′ and 5′-CATGTCCAG CAGCTAGTT-3′ for Cx43, 5′-ATAGACAGCATGAGAGG GAT-3′ and 5′-AGACAGGCATAGAATTAGGC-3′ for Cx26, 5′-CTTCCTTCCCTGGCTACTTC-3′ and 5′-CATCCC ATCTCTTGTACCCA-3′ for Cx32, 5′-GAGATCAGAGCCC AGGATGCT-3′ and 5′-CTGAGGGGTGGTGCCAAGGAG-3′

ID: sangeethag Date: 15/3/08 Time: 13:52 Path: J:/Production/JBMM/VOL00000/080132/3B2/C2JBMM080132

J_ID: ZA1 Customer A_ID: 07-0056.R1 Cadmus Art: JBMM32018 Date: 15-MARCH-08 Stage: I Page: 4

for nestin, 5′-TCCGCTGCTCGCCGCTCCTAC-3′ and 5′-TCAT CTCTGCCCGCTCACTGG-3′ for glial fibrillary acidic protein (GFAP), 5′-CACTTCCTCCTCCTCCACGAC-3′ and 5′-GTCCATGGCCAGGTTCAGGTC-3′ for oligodendrocyte transcription factor 1 (OLIG1), 5′-CTAAGGAGGA GATTGGACAGG-3′ and 5′-AGTGGTGGCAGTGATTTCA GT-3′ for Nurr-1, and 5′-ACCACAGTCCATGCCATCAC-3′ and 5′-TCCACCACCCTGTTGCTGTA-3′ for GAPDH. The RNA preparation and RT-PCR in this study were performed in triplicate.

Statistical analysis

Student's *t*-test was used to assess whether differences observed between the SHya-supplemented and control samples were statically significant. For comparison of groups of means, one-way analysis of variance was carried out. When significant differences were found, Tukey's pairwise comparison was used to investigate the nature of the difference. The confidence level was set at 95% for all tests. Statistical significance was accepted at $p < 0.05$. Values were presented as mean ± SD.

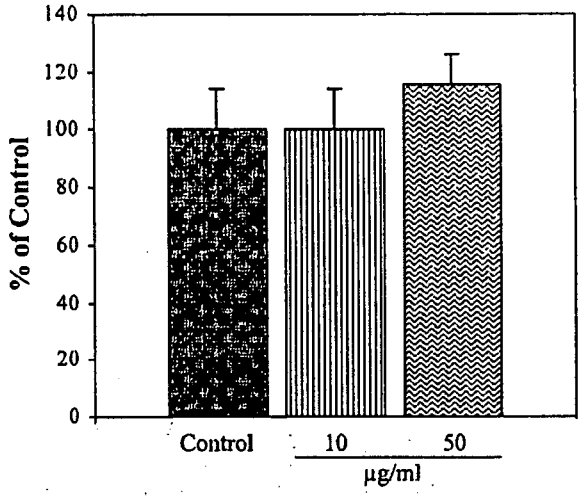

Figure 3. MTT assay for cell proliferation. Cell proliferation was nonsignificantly increased about 1.2-fold with 50 μg/mL SHya-treated cultures compared with control.

RESULTS AND DISCUSSION

NHA was cultured with different concentrations (10 and 50 μg/mL) of SHya. After 3 days and 1-week culture, cells were observed by inverted light microscopy observation and Giemsa staining. After 3-day culture, some cells looked like the branches or spikes extending out from the cell body (neuron) in control and 10 μg/mL of SHya-treated cultures, and the neurons were elongated and increased in number in 50 μg/mL of SHya-treated cultures [Fig. 2(A–C)]. After 1 week, in addition to neuron, some cells appeared like the sparse branches of a tree (oligodendrocyte) with 10 μg and 50 μg/mL of SHya. The number of oligodendrocytes was increased at 50 μg/mL of SHya-treated cultures, compared with the control culture [Fig. 2(D–F)]. Cell proliferation was nonsignificantly increased about 1.2-fold with 50 μg/mL SHya compared with control (Fig. 3) but was almost similar to control when treated with 10 μg/mL of SHya.

Astrocytes are coupled to a cellular network via gap junction channels predominantly composed of Cx43. Astrocytes are believed to play an important role in neuroprotection by providing energy substrates to neurons and by regulating the concentrations of K^+ and neurotransmitters via gap junctions. Therefore, we measured the GJIC function by SLDT assay. GJIC was significantly increased in cells cultured with SHya [Fig. 4(A,B)].

The expression of the Cx43 gene was also significantly increased in 50 μg/mL SHya-treated cultures [Fig. 5(A)]. It was reported that Cx26, Cx30, and Cx43 are expressed in astrocytes,[9] and Cx47 and Cx32 are expressed in oligodendrocytes; Cx32 is also expressed by neurons in mouse.[9,14] Astrocyte Cx26 is associated mainly with oligodendrocyte Cx32, whereas astrocyte Cx43 and Cx30 are associated with oligodendrocyte Cx47.[15] To evaluate their presence, we further estimated the expression levels of these specific genes. Expressions of Cx26 and Cx32 genes were increased in 50 μg/mL SHya-treated cultures about 4- and 3.5-fold, respectively, compared with the control culture [Fig. 5(B,C)]. In contrast, no expression of Cx30 and Cx47 genes was detected (data not shown). As mention earlier, mouse astrocyte and oligodendrocyte were capable to express Cx30 and Cx47 gene, respectively. But, in our experiment, we used human cell that failed to express these genes. We postulated that the difference in the species may play a vital role for the expression of these genes. Our data suggest that SHya promotes a strong association of astrocyte Cx26 with oligodendrocyte Cx32 and neuron Cx32.

The majority of cells in the CNS are generated during the embryonic and early postnatal period. Brain has long been regarded as incapable of regeneration. Therefore, discovery of new neurons in certain regions of adult mammalian brain has generated intense interest. Neural stem cells were reported to have the ability for expansion and differentiation into astrocytes, oligodendrocytes, and neurons *in vitro*.[16,17] It was suggested that a part of NHA have neural precursor activity that gives rise to astrocytes itself, oligodendrocytes and neurons, that express their original specific markers (Fig. 6).[18] Neural precursor cells express nestin, a class IV intermediate filament protein. Astrocytes express GFAP, a glial filamentous acidic protein. Oligodendrocytes express OLIG1, and differentiated neurons

ID: sangeethag Date: 15/3/08 Time: 13:52 Path: J:/Production/JBMM/VOL00000/080132/3B2/C2JBMM080132

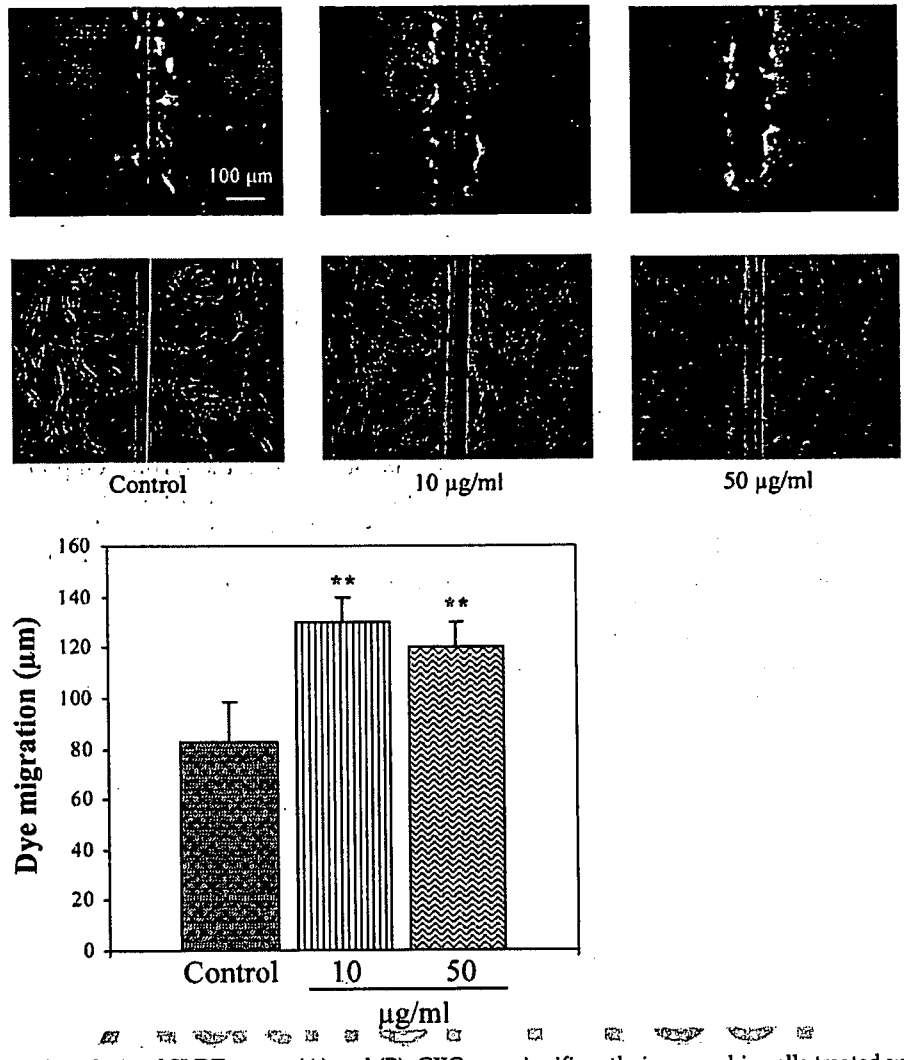

Figure 4. Statistical analysis of SLDT assay. (A) and (B), GJIC was significantly increased in cells treated with 10 and 50 μg/mL of SHya. $^{**}p < 0.01$. [Color figure can be viewed in the online issue, which is available at www.interscience.wiley.com.] AQ3

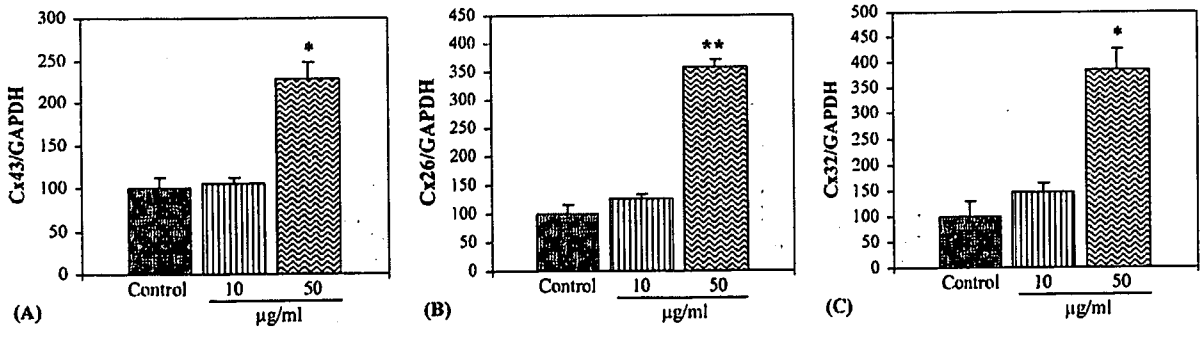

Figure 5. mRNA expression of Cx43, Cx26, and Cx32 by real-time PCR analysis. Expression of all gap junctional genes was significantly increased in 50 μg/mL SHya-treated cultures compared with control. (A) Expression of Cx43 was increased about 2.2-fold, (B) expression of Cx26 was increased about 4-fold, and (C) expression of Cx32 gene was increased about 3.5-fold. $^{*}p < 0.05$, $^{**}p < 0.01$.

J_ID: ZA1 Customer A_ID: 07-0056.R1 Cadmus Art: JBMM32018 Date: 15-MARCH-08 Stage: I Page: 6

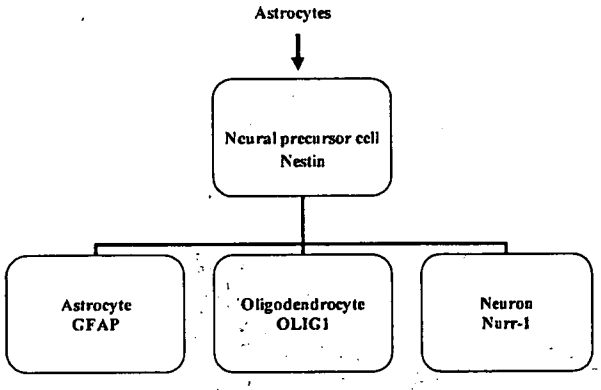

Figure 6. Schematic representation of astrocytes differentiation *in vitro*.

express Nurr-1, a transcription factor. In this study, we also determined the role of SHya in differentiation and expression of specific neural genes. When NHA was cultured with SHya, the expressions of nestin, GFAP, OLIG1, and Nurr-1 were significantly increased in 50 μg/mL SHya-treated cultures [Fig. F7 7(A–D)]. In all cases, the increases (about 2-, 3-, 1.8-, and 1.7-fold, respectively) were statistically significant at the concentration of 50 μg/mL SHya compared to the control. From this finding, it was suggested that astrocytes may be differentiated into neurons and/or oligodendrocytes with SHya-treated cultures.

Sulfated polysaccharides, such as heparan sulfate and heparin, are reported to mediate the activity of basic fibroblast growth factor in the ECM.[19] SHya, a semisynthetic material, composed of Hya and a sulfate group,[11] was synthesized by using Hya extracted from microorganisms; therefore, it has a lower infectivity and a lower risk of containing virus-induced carcinogens. Interaction of SHya with cells was already reported in several studies,[20] but the effect of SHya on cell proliferation, differentiation, and intercellular signaling was not clear. As reported earlier, SHya affected the osteoblasts responding to serum components supplied by FBS in the culture medium.[11] In our experiment, FBS was also added to the culture medium suggesting that SHya may affect cell function by interacting with the serum components. Moreover, Abatangelo et al.[21] reported SHya as a better nutrient for cells than Hya. Also, the SHya do not stimulate damage to the erythrocyte membrane. Therefore, we hypothesized a positive role of SHya on NHA.

CONCLUSION

In this study, we identified several distinct roles for SHya in NHA: increasing cell proliferation and facilitating GJIC function in a dose-dependent manner. Expressions of the specific markers of certain

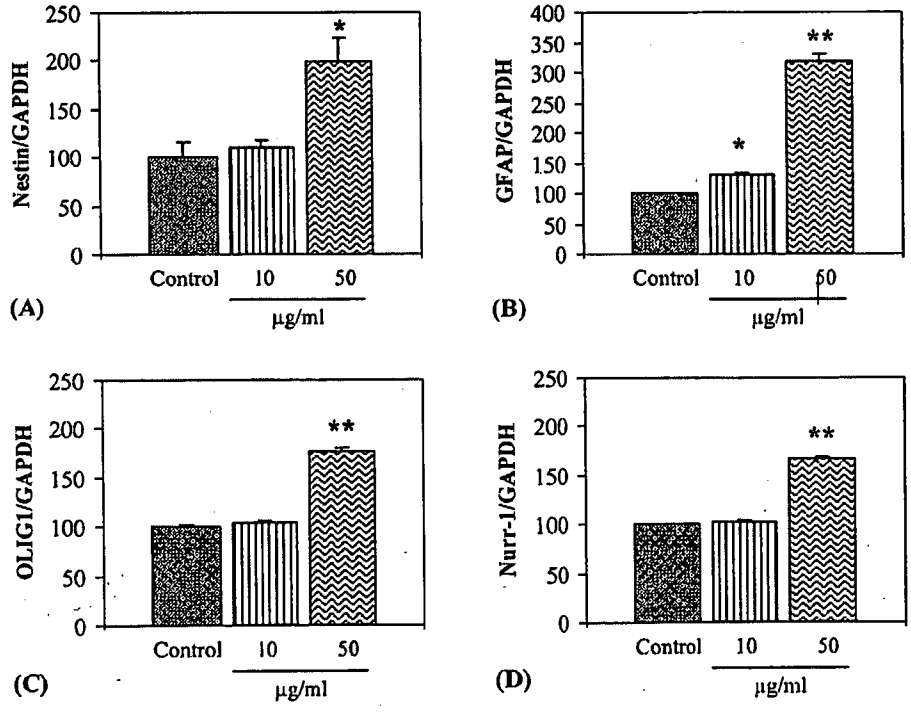

Figure 7. mRNA expression of neural cell marker genes by real-time PCR. The expressions of (A) Nestin, (B) GFAP, (C) OLIG1, and (D) Nurr-1 were increased. In all cases, at the concentration of 50 μg/mL, the increase was significant (about 2-, 3-, 1.8-, and 1.7-fold, respectively), compared to control. $^{*}p < 0.05$, $^{**}p < 0.01$.

ID: sangeethag Date: 15/3/08 Time: 13:52 Path: J:/Production/JBMM/VOL00000/080132/3B2/C2JBMM080132

genes were also enhanced with SHya treatment. Therefore, we postulate that SHya can bind with NHA and facilitate cell migration, adhesion, proliferation, and differentiation. Thus, SHya seems to play an important role in NHA and thus could help provide a novel material for the advancement of the field of tissue engineering.

References

1. McKay R. Stem cells in the central nervous system. Science 1997;276:66–71.
2. Gage FH. Mammalian neural stem cells. Science 2000;287: 1433–1438.
3. Rash JE, Staines WA, Yasumura T, Patel D, Furman CS, Stelmack GL, Nagy JI. Immunogold evidence that neuronal gap junctions in adult rat brain and spinal cord contain connexin-36 but not connexin-32 or connexin-43. Proc Natl Acad Sci U S A 2000;97:7573–7578.
4. Yeager M, Nicholson BJ. Structure of gap junction intercellular channels. Curr Opin Struct Biol 1996;6:183–192
5. Yeager M, Nicholson BJ. Structure and biochemistry of gap junctions. Adv Mol Cell Biol 2000;30:31–98.
6. Falk MM. Biosynthesis and structural composition of gap junction intercellular membrane channels. Eur J Cell Biol 2000;79:564–574.
7. Evans WH, Martin PE. Gap junctions: Structure and function (review). Mol Membr Biol 2002;19:121–136.
8. Bruzzone R, White TW, Paul DL. Connections with connexins: The molecular basis of direct intercellular signaling. Eur J Biochem 1996;238:1–27.
9. Nagy JI, Ionescu AV, Lynn BD, Rash JE. Coupling of astrocyte connexins Cx26, Cx30, Cx43 to oligodendrocyte Cx29, Cx32, Cx47: Implications from normal and connexin32 knockout mice. Glia 2003;44:205–218.
10. Bignami A, Hosley M, Dahl D. Hyaluronic acid and hyaluronic acid-binding proteins in brain extracellular matrix. Anat Embryol (Berl) 1993;188:419–433.
11. Nagahata M, Tsuchiya T, Ishiguro T, Matsuda N, Nakatsuchi Y, Teramoto A, Hachimori A, Abe K. A novel function of N-cadherin and Connexin43: Marked enhancement of alkaline phosphatase activity in rat calvarial osteoblast exposed to sulfated hyaluronan. Biochem Biophys Res Commun 2004; 315:603–611.
12. Anderegg G, Flaschka H, Sallmann R, Schwarzenbach G. Metallindikatoren VII. Ein auf Erdalkaliionen ansprechendes Phatalein und sein analytische Verwendung. Helv Chim Acta 1954;37:113–120.
13. El-Fouly MH, Trosko JE, Chang CC. Scrape-loading and dye transfer. A rapid and simple technique to study gap junctional intercellular communication. Exp Cell Res 1987;168: 422–430.
14. Nagy JI, Ionescu AV, Lynn BD, Rash JE. Connexin29 and connexin32 at oligodendrocyte and astrocyte gap junctions and in myelin of the mouse central nervous system. J Comp Neurol 2003;464:356–370.
15. Altevogt BM, Paul DL. Four classes of intercellular channels between glial cells in the CNS. J Neurosci 2004;24:4313–4323.
16. Johansson CB, Momma S, Clarke DL, Risling M, Lendahl U, Frisen J. Identification of a neural stem cell in the adult mammalian central nervous system. Cell 1999;96:25–34.
17. Reynolds BA, Weiss S. Generation of neurons and astrocytes from isolated cells of the adult mammalian central nervous system. Science 1992;255:1707–1710.
18. Reynolds BA, Weiss S. Clonal and population analyses demonstrate that an EGF- responsive mammalian embryonic CNS precursor is a stem cell. Dev Biol 1996;175:1–13.
19. Walker A, Turnbull JE, Gallagher JT. Specific heparan sulfate saccharides mediate the activity of basic fibroblast growth factor. J Biol Chem 1994;269:931–935.
20. Hollander D, Stein M, Bernd A, Windolf J, Wagner R, Pannike A. Autologous keratinocyte culture on hyaluronic acid ester membrane: an alternative in complicated wound management? Unfallchirurgie 1996;22:268–272.
21. Abatangelo G, Barbucci R, Brun P, Lamponi S. Biocompatibility and enzymatic degradation studies on sulphated hyaluronic acid derivatives. Biomaterials 1997;18:1411–1415.

AQ1: Kindly check whether the short title is OK as given.

AQ2: Per scientific convention, symbols/characters representing genes are set in italic while the same are set normally (in roman) when they represent proteins. Kindly indicate with an underline (in the proofs) all symbols/characters that represent genes.

AQ3: Please confirm whether the color figures should be reproduced in color or black and white in the print version. If the color figures must be reproduced in color in the print version, please fill the color charge form immediately and return to neuprod@wiley.com Or else, the color figures for your article will appear in color in the online version only.

J Artif Organs (2007) 10:22–28
DOI 10.1007/s10047-006-0363-y

ORIGINAL ARTICLE

Masato Tamai, PhD · Kazuo Isama
Ryusuke Nakaoka, PhD · Toshie Tsuchiya, PhD

Synthesis of a novel β-tricalcium phosphate/hydroxyapatite biphasic calcium phosphate containing niobium ions and evaluation of its osteogenic properties

Abstract To promote the osteogenic properties of osteoblasts, we synthesized a hydroxyapatite (HAp) with β-tricalcium phosphate (β-TCP) biphasic calcium phosphate containing Nb ions (NbTCP/HAp). NbTCP/HAp was prepared by annealing precipitates obtained by coprecipitation of an aqueous solution of $Ca(NO_3)_2$ and a mixture of $(NH_4)_2HPO_4$ and aqueous Nb solution. The precipitates can be regarded as a calcium-deficient HAp, the PO_4 sites of which are partly occupied by Nb ions. NbTCP/HAp was successfully synthesized by thermal decomposition of the precipitates. NbTCP/HAp enhanced the calcification of normal human osteoblasts (NHOst), and the amount of calcified tissue increased in proportion to the Nb ion concentration in the NbTCP/HAp. The alkaline phosphatase (ALP) activity of NHOst was also enhanced by NbTCP/HAp. Because Nb ions significantly enhance the ALP activity of NHOst, calcification by NbTCP/HAp is considered to be due to enhancement of ALP activity induced by Nb ions dissolved from NbTCP/HAp. These results indicate that NbTCP/HAp can be an effective bone repair material.

Key words Tissue engineering · Bone · Osteoblasts · Calcium phosphate · Nb ions

Introduction

Bone tissue engineering offers a promising alternative strategy for healing severe bone injuries by utilizing the body's natural biological response to tissue damage in conjunction with engineering principles. Osteogenic cells, growth factors, and biomaterial scaffolds form the foundation of the many bone tissue engineering strategies employed to achieve regeneration of damaged bone tissue. An ideal biomaterial scaffold will provide mechanical support to an injured site and also enhance osteogenic differentiation to encourage bone growth.[1] To develop biomaterial scaffolds with optimal performance, understanding the interactions between osteoblasts and scaffolds is extremely important.

Hydroxyapatite [HAp, $Ca_{10}(PO_4)_6(OH)_2$] and related calcium phosphate ceramics, e.g., β-tricalcium phosphate [β-TCP, β-$Ca_3(PO_4)_2$], have good biocompatibility with bone tissue because their chemical compositions are very similar to the mineral phase of human bone. It is well known that these calcium phosphate ceramics can be biologically bonded to natural bone. In fact, it has been reported that porous materials composed of HAp, β-TCP, or β-TCP/HAp biphasic calcium phosphate are useful for bone tissue regeneration because of their osteoconductivity.[2–6] It has also been reported that β-TCP/HAp biphasic calcium phosphate shows better osteoconductivity than HAp or β-TCP alone.[7,8] Therefore, this material has been actively studied for use as a scaffold for bone tissue regeneration.

In a previous study, Nb ions were reported to lower cytotoxicity[9] (IC_{50} of Nb ions for L929 fibroblasts is 3.63×10^3), and we reported that Nb ions significantly promoted the calcification of normal human osteoblasts (NHOst).[10] Furthermore, we succeeded in synthesizing a hydroxyapatite containing Nb ions (NbHAp) and showed that NbHAp has the potential to promote alkaline phosphatase (ALP) activity, an important factor in the generation of new bone, in NHOst.[11] In this study, to further promote the cell activity of osteoblasts, we synthesized β-TCP/HAp biphasic calcium phosphate containing Nb ions and investigated interactions between β-TCP/HAp biphasic calcium phosphate and NHOst in vitro.

Materials and methods

Synthesis and characterization of β-TCP/HAp biphasic calcium phosphate containing Nb ions

Reagent grade $Ca(NO_3)_2$, $(NH_4)_2HPO_4$, and $NbCl_5$ (Wako, Osaka, Japan) were used without purification. NbTCP/HAp

Received: May 26, 2006 / Accepted: September 28, 2006

M. Tamai · K. Isama · R. Nakaoka · T. Tsuchiya (✉)
Division of Medical Devices, National Institute of Health Sciences,
1-18-1 Kamiyoga, Setagaya-ku, Tokyo 158-8501, Japan
Tel. +81-3-3700-4842; Fax +81-3-3707-6950
e-mail: tsuchiya@nihs.go.jp

samples were prepared by annealing precipitates obtained from coprecipitation of an aqueous solution of $Ca(NO_3)_2$ with a mixture of $(NH_4)_2HPO_4$ and an aqueous solution of Nb as described below. $Ca(NO_3)_2$ and $(NH_4)_2HPO_4$ were completely dissolved in distilled water. The aqueous Nb solution was prepared by mixing distilled water and $NbCl_5$ dissolved in 5% hydroxyacetone and 5% 2-aminoethanol.[12] A 0.2 M $(NH_4)_2HPO_4$ aqueous solution was combined with 0.01 M $NbCl_5$ and stirred with a magnetic bar at Nb/(Nb + P) molar ratios of 0.0000, 0.0167, or 0.1667. The pH of the mixture was adjusted to 10 using 1 N NaOH throughout the reaction, and 0.2 M $Ca(NO_3)_2$ was slowly dropped into the mixture (20 ml/min). The amount of 0.2 M $Ca(NO_3)_2$ solution was adjusted to a Ca/(Nb + P) molar ratio of 1.6 in order to synthesize β-TCP/HAp biphasic calcium phosphate, followed by stirring the suspension for 24 h at room temperature. The precipitates were centrifuged at 3600 rpm for 5 min and washed with distilled water. The resulting precipitates of Nb/(Nb + P) with molar ratios of 0.0000, 0.0167, and 0.1667 were named NbHAp-0, NbHAp-I, and NbHAp-II, respectively. These precipitates were then annealed at 800°C for 2 h (temperature increase: 5°C/min) and named NbTCP/HAp-0, NbTCP/HAp-I, and NbTCP/HAp-II, respectively. The NbTCP/HAp samples obtained were characterized by X-ray diffraction analysis (XRD, Rint2000, Rigaku, Tokyo, Japan) with Cu K_α radiation (40 kV, 50 mA). The XRD profiles of 2θ angles between 20° and 60° with a step interval of 0.01° were collected at a scanning rate of 4°/min. Also, measurement of the lattice parameter was carried out using the 211, 112, and 300 planes of HAp, and data for the lattice parameter were collected with a scan rate of 0.025°/min. The observed interplanar spacing was corrected using elemental Si as a standard material.

Concentrations of Ca, P, and Nb ions in the precipitate were estimated by inductively coupled plasma analysis (ICP, HP4500, Hewlett-Packard, CA, USA) after the precipitate was dissolved in HNO_3 solution. Microstructural evaluation of the precipitates was performed by scanning electron microscopy (SEM, JSM-5800LV, JEOL, Tokyo, Japan; acceleration voltage: 25 kV) and energy-dispersive X-ray spectroscopy (EDX) (LV5800, JEOL).

Osteogenic effects of NbTCP/HAp

NbTCP/HAp pellets were fabricated to investigate their effects on the osteogenic function of osteoblasts. In total, 100 mg of powdered NbTCP/HAp was put into a stainless steel mold and uniaxially pressed at 30 MPa for 1 min to form a pellet 0.5 mm in thickness and 12 mm in diameter. The pellets were sintered at 800°C for 2 h (temperature increase: 5°C/min).

NHOst were purchased from BioWhittaker (Walkersville, MD, USA) and maintained in d-minimumessential medium (αMEM) (Gibco, Grand Island, NY, USA) containing 10% fetal calf serum (FCS, Kokusai Sinyakyu, Tokyo, Japan) in incubators at 37°C in a humid atmosphere with 5% CO_2. All assays were performed using αMEM containing 10% FCS supplemented with 10 mM β-glycerophosphate.

Cells were seeded on the pellets as described below. Each NbTCP/HAp pellet was immersed in 1 ml culture medium in a well of a 24-well cell culture plate (Corning, Corning, NY, USA) and incubated at 37°C for 24 h. After discarding the medium, 300 μl of new culture medium was put into each well, followed by 1 ml of NHOst suspension (4×10^4 cell/ml), and incubation was carried out for 4 h. Finally, the cell-seeded NbTCP/HAp pellet was transferred to a new well of a 24-well plate with 1 ml of the test medium and incubated at 37°C in a humidified atmosphere with 5% CO_2 for 7–14 days.

Extracts from various NbTCP/HAp samples were prepared to investigate their effects on dissolved ions. NbTCP/HAp powder (100 mg/ml) was added to the culture medium (αMEM) containing 10% FCS and immersed at 37°C for 24 h. After changing the medium, the suspensions were stirred by a shaker at 200 rpm for 72 h at 37°C. The suspension was centrifuged at 3600 rpm for 5 min, and the supernatant was collected to use as an extract for an osteogenesis test in vitro. The atomic concentrations of Nb in the extract were measured by ICP.

An NHOst suspension (4×10^4 cells/ml) was added to culture wells and incubated for 4 h. After the NHOst had adhered to the well, the suspension medium was discarded and 1 ml of the extract supplemented with 10 mM β-glycerophosphate was added. The NHOst were incubated at 37°C in a saturated humid atmosphere with 5% CO_2 for 7–14 days.

We also examined the effect of Nb ions on the osteogenesis of NHOst. A solutionn of 0.2 μM $NbCl_5$/αMEM and serial dilutions were prepared. In addition to the experiment using the extracts indicated above, NHOst were cultured in $NbCl_5$/αMEM supplemented with β-glycerophosphate for 7–14 days.

Proliferation of NHOst cells in each experiment was estimated by a TetraColor One assay (Seikagaku, Tokyo, Japan), which incorporates an oxidation–reduction indicator based on detection of metabolic activity. After a 7-day incubation, the culture medium was discarded and 2% TetraColor One/αMEM solution was added to each well and was incubated for 2 h. The absorbance of the supernatant at 450 nm was measured using a μQuant spectrophotometer (Bio-tek, Winooski, VT, USA) to estimate the proliferation of the test cells. After estimating the proliferation, the cells were washed with phosphate-buffered saline [PBS(–)], followed by the addition of 1 ml of 0.1 M glycine buffer (pH 10.5) containing 10 mM $MgCl_2$, 0.1 mM $ZnCl_2$, and 4 mM *p*-nitrophenylphosphate sodium salt. The absorbance of the added buffer at 405 nm after 5 min incubation at room temperature was detected to evaluate the ALP activity of the test cells. After measurement of ALP, the NHOst cultured in the extract were washed with PBS(–) three times and the calcium phosphate deposited by NHOst was estimated. The amount of deposited calcium phosphate dissolved in 0.1 N HCl solution was determined by a Wako Calcium C test kit (Wako), which is based on the *o*-cresolphthalein complex color development method. The NHOst in all assays were stained in 5% Giemsa solution and observed by light microscopy (Nikon, Eclipse TE300, Tokyo, Japan) to confirm

Table 1. Chemical composition and characteristics of the precipitates prepared in this study

Sample	Phase	Annealing temperature	Theoretical composition[a]		Measured composition[a]		Color of precipitate	Lattice parameter[b]	
			Ca/(P + Nb)	Nb/(P + Nb)	Ca/(P + Nb)	Nb/(P + Nb)		*a*-axis (nm)	*c*-axis (nm)
NbHAp-0	HAp		1.60	0.000	1.60	–	White	–	–
NbHAp-I	HAp		1.60	0.017	1.56	0.013	Pale yellow	–	–
NbHAp-II	HAp		1.60	0.167	1.56	0.077	Buff yellow	–	–
NbTCPHAp-0	β-TCP + HAp	800°C	1.60	0.000	1.60	–	White	0.939	0.687
NbTCP/HAp-I	β-TCP + HAp	800°C	1.60	0.017	1.56	0.013	White	0.942	0.689
NbTCP/HAp-II	β-TCP + HAp	800°C	1.60	0.167	1.56	0.074	White	0.943	0.690

HAp, hydroxyapatite; NbHAp, hydroxyapatite containing Nb ions; TCP, tricalcium phosphate

[a] Molar ratio

[b] Lattice parameter for HAp

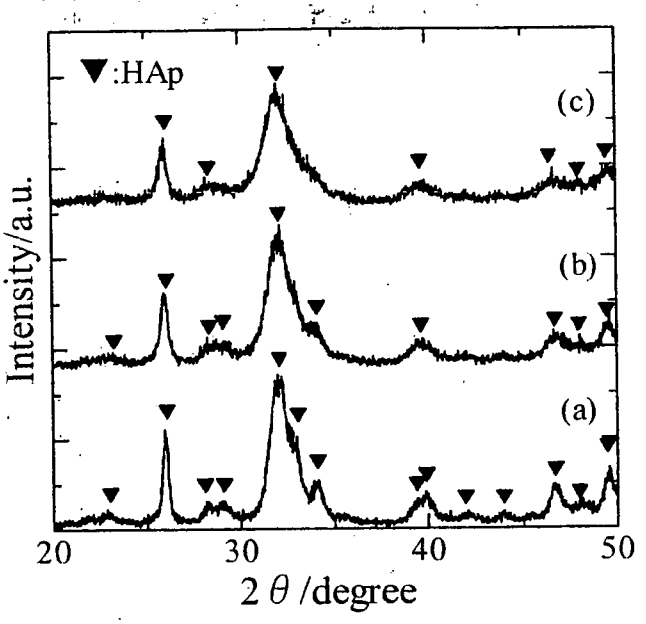

Fig. 1. X-ray diffraction (XRD) patterns of the precipitates with a Ca/(P + Nb) molar ratio of 1.50: *a*, Nb/(Nb + P) = 0; *b*, Nb/(Nb + P) = 0.0167; and *c*, Nb/(Nb + P) = 0.1667. *Triangles* represent XRD peaks due to the crystal structure of hydroxyapatite (HAp)

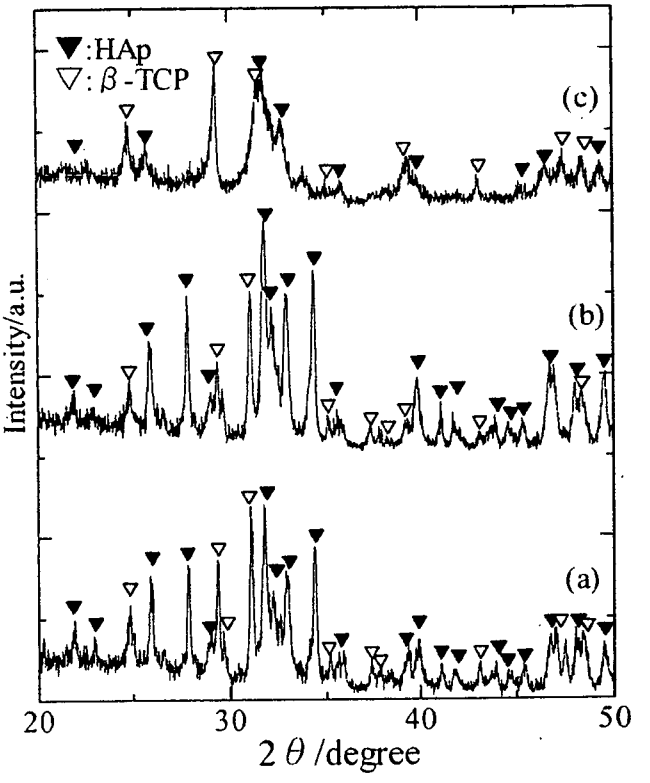

Fig. 2. XRD patterns of the annealed precipitates with a Ca/(P + Nb) molar ratio of 1.50: *a*, Nb/(Nb + P) = 0; *b*, Nb/(Nb + P) = 0.0167; and *c*, Nb/(Nb + P) = 0.1667. These precipitates were annealed at 800°C. *β-TCP*, β-tricalcium phosphate

their proliferation. All results were expressed as mean values ± SD and were analyzed statistically with Student's *t* test.

Results

XRD patterns of the precipitates prepared in this study are shown in Fig. 1. The XRD indicated that precipitates with Nb/(Nb + P) molar ratios from 0 to 0.167 had a monolithic apatite structure, irrespective of the Nb/(Nb + P) molar ratio of the starting solution, although the level of crystallite decreased as the Nb content increased. XRD patterns of the precipitates with various Nb/(Nb + P) molar ratios annealed at 800°C are shown in Fig. 2. The level of crystallites of the precipitates was high due to the annealing, and their diffraction peaks were composed of those of both HAp and β-TCP. Interestingly, the crystallite level decreased when the Nb level increased.

The chemical compositions and characteristics of the precipitates prepared in this study are summarized in Table 1. Both the Ca/(Nb + P) and the Nb/(P + Nb) molar ratios in precipitates measured by ICP approximately agreed with their theoretical values, except for the Nb/(P + Nb) molar ratio of NbTCP/HAp-II: the measured Nb/(P + Nb) molar ratio of NbTCP/HAp-II was 0.074, which is lower than the theoretical value of 0.167. The lattice parameter of the HAp phase in NbTCPHAp increased with increasing Nb content.

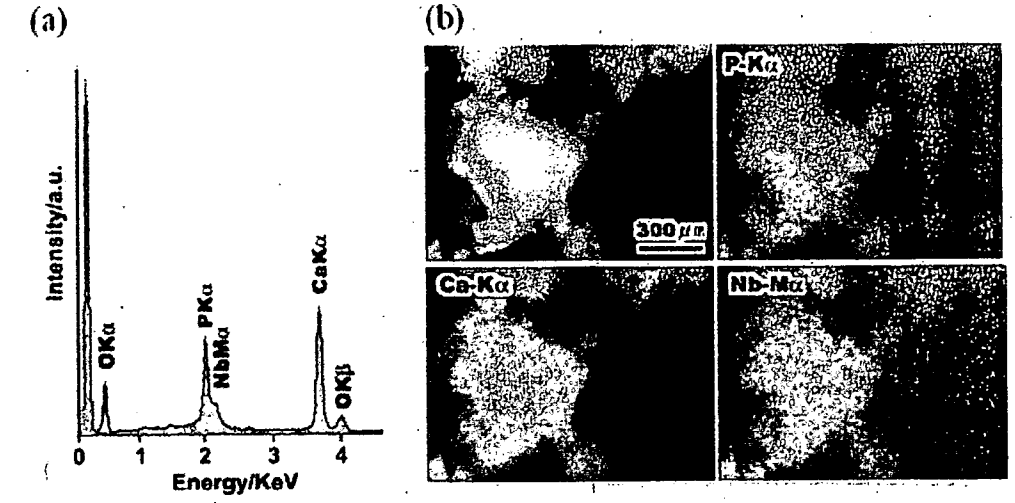

Fig. 3. Scanning electron microscopy–energy-dispersive X-ray spectroscopy spectra of NbTCP/HAp-II annealed at 800°C (**a**) and their mapping images from P-Kα, Ca-Kα, and Nb-Mα lines (**b**)

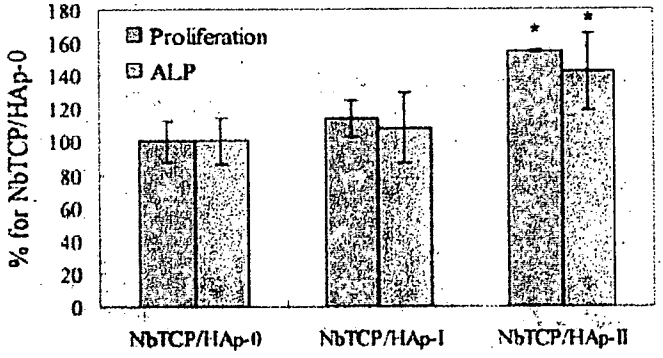

Fig. 4. Proliferation and alkaline phosphatase (*ALP*) activity of normal human osteoblasts (NHOst) cultured on various kinds of NbTCP/HAp pellets. $*P < 0.01$ against NbTCP/HAp-0 (without Nb ions)

The lattice parameters of NbTCP/HAp-0 without Nb ions were 0.939 nm for the *a*-axis and 0.687 nm for the *c*-axis, while those of NbTCP/HAp-II were 0.943 nm for the *a*-axis and 0.690 nm for the *c*-axis. In addition, the color of the precipitates became dark yellow as the Nb/(P + Nb) molar ratio increased, while the annealed precipitates of NbTCP/HAp were white.

SEM observation of the precipitates before annealing revealed that all precipitates were present as aggregates composed of primary particles of less than 1 μm in diameter, irrespective of the Nb/(P + Nb) molar ratio. Figure 3a shows SEM-EDX spectra of NbTCP/HAp-II. The EDX spectrum of Nb Mα was separated from the P K_α line and could be observed at 2.17 KeV, although its intensity was weak. The mapping images of the P-K_α, Ca-K_α, and Nb-M_α lines are shown in Fig. 3b. As shown in Fig. 3b, Nb ions were present at the same site as the Ca and P ions, suggesting that the Nb ions were homogenously distributed in the aggregates.

The proliferation and ALP activity of NHOst cultured on various kinds of NbTCP/HAp pellets is shown in Fig. 4. The proliferation of NHOst cultured on NbTCP/HAp-II pellets was approximately 60% higher than that on NbTCP/HAp-0 without Nb ions ($P < 0.01$). As shown in Fig. 5, many

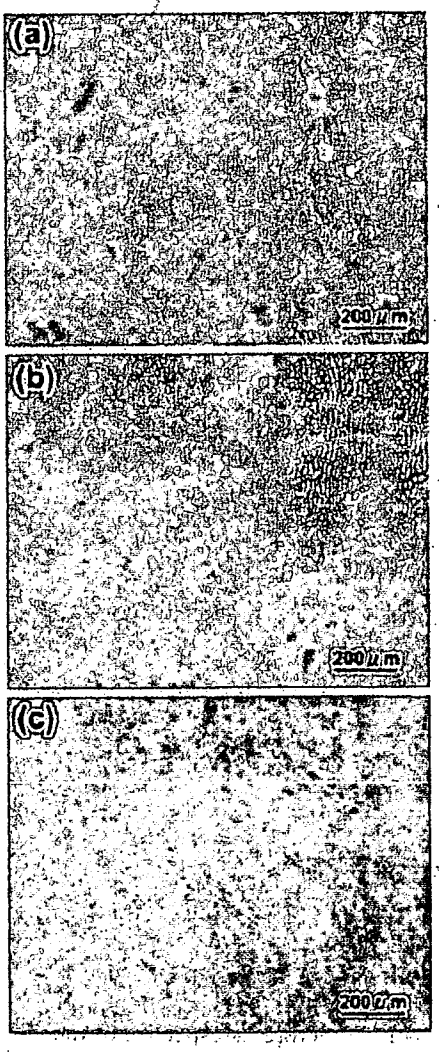

Fig. 5. Light microscopic images of NHOst cultured on various NbTCP/HAp samples for 7 days: *a*, NbTCP/HAp-0; *b*, NbTCP/HAp-I; and *c*, NbTCP/HAp-II. NHOst were stained by Giemsa solution

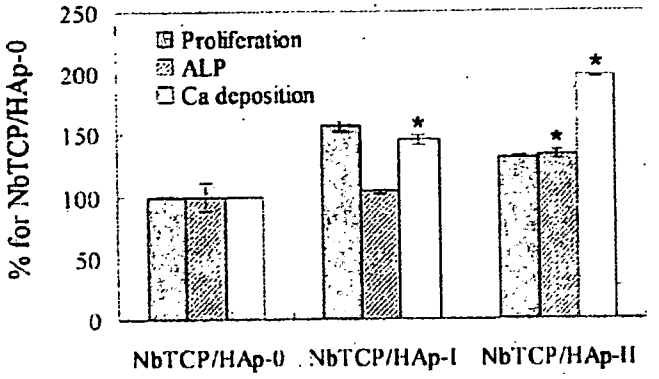

Fig. 6. Osteogenic properties (proliferation, ALP activity, and Ca deposition) of NHOst cultured in extracts from various NbTCP/HAp samples for 14 days. *$P < 0.01$ against NbTCP/HAp-0 (without Nb ions)

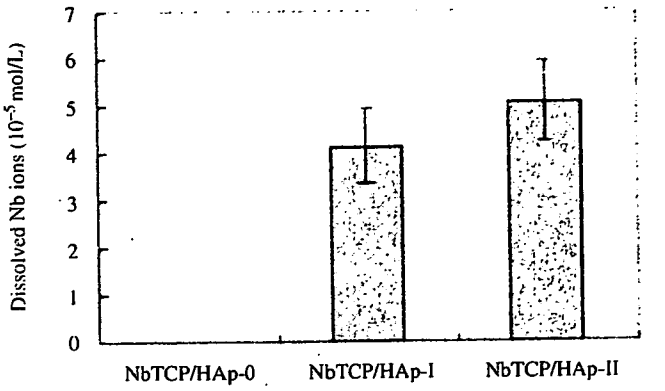

Fig. 7. Concentrations of Nb ions in extracts from various NbTCP/HAp samples. The concentration of Nb ions in cell culture medium was measured by inductively coupled plasma analysis

NHOst adhered to and spread on NbTCP/HAp-I and -II, while little spreading of NHOst was observed on HAp. In addition, as shown in Fig. 4, NHOst cultured on the NbTCP/HAp-II pellets expressed high ALP activity, compared with those cultured on NbTCP/HAp-0. Figure 6 shows the proliferation, ALP activity, and Ca deposition of NHOst cultured in extracts from various NbTCP/HAp samples for 14 days. Like the NHOst cultured on pellets, NHOst cultured in the extract from NbTCP/HAp-II expressed higher ALP activity than those in the extract from NbTCP/HAp-0. Furthermore, the amount of deposited calcium from NHOst increased with increasing Nb ion concentration in NbTCP/HAp, and the calcium deposition in the extract from NbTCP/HAp-II was twice that in the extract from NbTCP/HAp-0.

Figure 7 shows the concentration of Nb ions in extracts from NbTCP/HAp samples. It was found that Nb ions were released into the cell culture medium at concentrations of the order of 1×10^{-5} mol/l. To investigate the effect of Nb ions on NHOst function, NHOst were cultured in a medium containing Nb ions. The dependence of osteogenesis by NHOst on Nb ion concentration is shown in Fig. 8. Nb ions did not affect the proliferation of NHOst, but the ALP activity and Ca deposition of NHOst proceeded proportionally when the concentration of Nb ions was more than 1×10^{-5} mol/L.

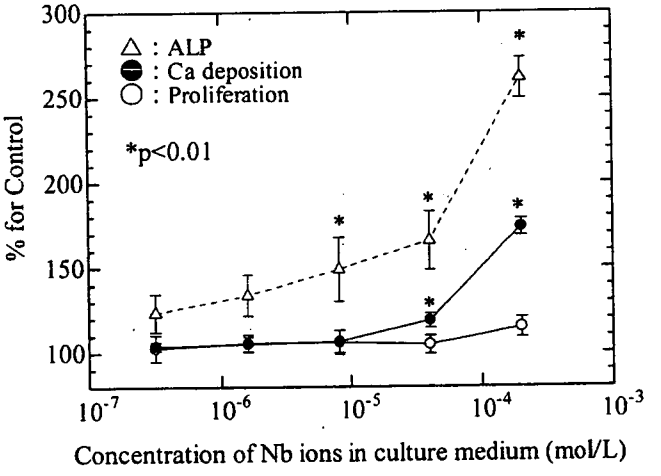

Fig. 8. Relationship between concentration of Nb ions in culture medium and osteogenic properties of NHOst. *$P < 0.01$ against cell culture medium without Nb ions

Discussion

Characterization of NbTCP/HAp biphasic calcium phosphate ceramics

As summarized in Table 1, before annealing the precipitates, the NbHAp samples were hydroxyapatite with low levels of crystallite. The hydroxyapatite structure is known to be very tolerant of ionic substitution.[12] Ca^{2+} ions, PO_4^{3-} ions, and OH^- ions can be replaced, partly or completely, by various cationic or anionic ions. Notably, as shown in Table 1, the lattice parameter of HAp increased when the Nb content in NbTCP/HAp was high. This fact suggests that Nb ions are taken into the apatite lattice. If a substitution of an Nb^{5+} ion for a Ca^{2+} ion in HAp occurred, the lattice parameter should decrease, since the ionic radius of Ca^{2+} and Nb^{5+} are 0.1 nm and 0.064 nm, respectively. Therefore, the possibility of substitution of Nb ions for Ca ions is low. On the other hand, although the structure of Nb ions in aqueous solution is not fully understood at present, it has been reported that Nb ions in solution are not present as Nb^{5+} but as niobiumate acid, $H_xNb_6O_{19}^{(8-x)-}$ ions (x = 0,1,2) for basic conditions,[14,15] and the niobiumate acid cluster ($H_xNb_6O_{19}^{(8-x)-}$) was polymerized or dissociated depending on the pH and ion concentration.[15] According to these reports, $H_4NbO_6^{3-}$ anionic monomer can exist in basal and low Nb concentrations (<0.08 M). Since the Nb concentration in this study was 0.01 M, Nb ions would exist as $H_4NbO_6^{3-}$ anionic monomers. $H_4NbO_6^{3-}$ may be substituted at the PO_4 site since the PO_4 site in HAp can be replaced by anionic

atomic groups. In addition, the ionic radius of the $H_4NbO_6^{3-}$ monomer and PO_4 are approximately 0.30 nm and 0.23 nm, respectively, suggesting that an increase in lattice parameter of NbTCP/HAp is ascribed to the substitution of PO_4 sites by this monomer in HAp. Furthermore, the fact that both the Ca/(Nb + P) and Nb/(P + Nb) molar ratios of the precipitates, as measured by ICP, approximately agreed with their theoretical values may support this hypothesis. Despite the theoretical Nb/(Nb + P) ratio being 0.1667, the Nb/(Nb + P) molar ratio in NbTCP/HAp-II was about 0.07, which suggests that the maximum amount of substituted Nb ions at the PO_4 site is around 0.07.

The Ca/(P + Nb) molar ratio in the NbHAp obtained in this study was lower than that of the stoichiometric value of 1.67 for HAp. Hydroxyapatite having a lower Ca/P molar ratio is known as calcium-deficient hydroxyapatite [Ca-def HAp, $Ca_{10-Z}(HPO_4)_Z(PO_4)_{6-Z}(OH)_{2-Z}$, $Z = 0–1$]. Therefore, NbHAp can be regarded as a Ca-def HAp in which the PO_4 sites are partly occupied by Nb ions.

Ca-def HAp decomposes to stoichiometric HAp and β-TCP at temperatures above 600°C according to the following reaction:[16,17]

$$Ca_{10-Z}(HPO_4)_Z(PO_4)_{6-Z}(OH)_{2-Z}\cdot nH_2O \rightarrow (1-Z)Ca_{10}(PO_4)_6(OH)_2 + 3Z\cdot\beta\text{-}Ca_3(PO_4)_2 + Z\cdot nH_2O$$

The above thermal decomposition reaction occurred during the annealing of NbHAp, resulting in a lower Ca/P molar ratio than the stoichiometric value of HAp because of partial β-TCP formation. In addition, the homogenously distributed Nb ions in NbTCP/HAp may result from thermal diffusion of Nb ions during the thermal decomposition process.

Osteogenesis of NHOst cultured on NbTCP/HAp

In this study, NbTCP/HAp showed potential to promote calcification of NHOst. This study indicated that osteogenic behavior of NHOst cultured on NbTCP/HAp pellets was consistent with that of NHOst cultured in extracts from the pellets, suggesting that dissolved ions from the NbTCP/HAp pellets affect calcification of NHOst. As shown in Fig. 7, Nb ions were apparently released from NbTCP/HAps and dissolved in the medium at concentrations of the order of 1×10^{-5} mol/l. When 4×10^{-5} mol/l of $NbCl_5$ was added to the culture medium, Ca deposition clearly increased (Fig. 8). Therefore, the enhancement of Ca deposition is considered to be due to the dissolved Nb ions. One possible mechanism for enhancement of calcification is discussed below.

ALP is known to play an important role in the calcification of bone.[18–20] Generally, the calcification of bone mineral occurs in the matrix vesicles budding from the surface of osteoblasts.[21] The nucleation of biological apatite, which is the initial stage of calcification, occurs due to the reaction between inorganic PO_4^{3-} ions produced by the ALP and calcium ions in matrix vesicles.

NHOst cultured on the NbTCP/HAp pellets containing Nb ions expressed high ALP activity compared with those cultured on HAp without Nb ion. Similarly, it was found that NHOst cultured in an extract from NbTCP/HAp containing Nb ions expressed higher ALP activity than those in the extract from HAp without Nb ions. These results suggest that Nb ions affect the enhancement of ALP activity. Based on the above calcification mechanism in matrix vesicles, the enhancement of calcification might result from the enhancement of ALP activity due to dissolved Nb ions from NbTCP/HAp. The enhancement of ALP activity increases the production of inorganic PO_4^{3-} ions, and then the inorganic PO_4^{3-} ions produced may be taken into the matrix vesicles. The subsequent nucleation of biological hydroxyapatite occurs due to a reaction of Ca ions and inorganic PO_4^{3-} ions, followed by calcification. Although we cannot deny that Nb ions directly promote calcification by NHOst unrelated with ALP expression, the essence of the calcification enhancement by NbTCP/HAp may be the enhancement of ALP activity by Nb ions dissolved from NbTCP/HAp. The biological effect of Nb ions on NHOst is under investigation. Although further studies are necessary to clarify the mechanism of enhanced calcification by Nb ions, this study strongly suggests that NbTCP/HAp is a more promising material for use as a bone tissue engineering scaffold than HAp.

Conclusion

In order to promote the osteogenicity of osteoblasts, we synthesized a combination of HAp and β-TCP biphasic calcium phosphate containing Nb ions (NbTCP/HAp). The NbTCP/HAp samples were prepared by annealing precipitates obtained by coprecipitation of an aqueous solution of $Ca(NO_3)_2$ with a mixture of $(NH_4)_2HPO_4$ and aqueous Nb solution. The precipitates obtained by the coprecipitation process can be identified as Ca-def HAp, the PO_4 sites of which are partly occupied by Nb ions. NbTCP/HAp samples were successfully obtained by thermal decomposition of the precipitates.

NbTCP/HAp enhanced calcification of NHOst. The enhancement of calcification of NbTCP/HAp was ascribed to the enhancement of ALP activity due to the dissolved Nb ions from NbTCP/HAp.

Acknowledgments This study was supported in part by a Grant-in-Aid for Scientific Research on Advanced Medical Technology from the Ministry of Labour, Health and Welfare of Japan, and a Grant-in-Aid from the Japan Health Sciences Foundation.

References

1. Service FR. Tissue engineers build new bone. Science 2000;289: 1498–1500
2. Tamai N, Myoui A, Tomita T, Nakase T, Tanaka J, Ochi T, Yoshikawa H. Novel hydroxyapatite ceramics with an interconnective porous structure exhibit superior osteoconduction in vivo. J Biomed Mater Res 2002;59:110–117
3. Ohgushi H, Goldberg VM, Caplan IA. Heterotopic osteogenesis in porous ceramics induced by marrow cells. J Orthop Res 1989;7: 568–578

4. Cheung SH, Haak HM. Growth of osteoblasts on porous calcium phosphate ceramic: an in vitro model for biocompatibility study. Biomaterials 1989;10:63–67
5. Uchida A, Nade S, McCartney E, Ching W. Growth of bone marrow cells on porous ceramics in vitro. J Biomed Mater Res 1987;21: 1–10
6. Ohgushi H, Okumura M. Osteogenic capacity of rat and human marrow cells in porous ceramics. Acta Orthop Scand 1990;61: 431–434
7. Schopper C, Ziya-Ghazvini F, Goriwoda W, Moser D, Wanschitz F, Spassova E, Lagogiannis G, Auterith A, Ewers R. HA/TCP compounding of a porous CaP biomaterial improves bone formation and scaffold degradation – a long term histological study. J Biomed Mater Res B 2005;74B:458–467
8. Yuan H, Van DDM, Shihong L, Groot BV, Bruijn DDJ. A comparison of the osteoinductive potential of two calcium phosphate ceramics implanted intramuscularly in goats. J Mater Sci Mater Med 2002;13:1271–1275
9. Yamamoto A, Honma R, Sumita M. Cytotoxicity evaluation of 43 metal salts using murine fibroblast and osteoblastic cells. J Biomed Mater Res 1998;39:331–340
10. Isama K, Tsuchiya T. Bull Natl Inst Health Sci 2003;121:111
11. Tamai M, Nakaoka R, Isama K, Tsuchiya T. Novel calcium phosphate ceramics: the remarkable promoting action on the differentiation of normal human osteoblasts. Key Eng Mater 2006; 309–311:97–100
12. Ohya T, Ban T, Ohya Y, Takahashi Y. Preparation of concentrated, halogen-free aqueous titanium solution. Ceram Trans 2001;112: 47–52
13. Elliott CJ. Structure and chemistry of the apatites and other calcium orthophosphates. Tokyo: Elsevier, 1994
14. Cotton AF, Wilkinson G. Advanced inorganic chemistry. Tokyo: Baifukan, 1994
15. Jehng JM, Wachs IE. Niobium oxide solution chemistry. J Raman Spec 1991;22:83–89
16. Tamai M, Nakamura M, Isshiki T, Nishio K, Endoh H, Nakahira A. A metastable phase in thermal decomposition process of Ca-deficient hydroxyapatite. J Mater Sci Mater Med 2003;14: 617–622
17. Gibson IR, Rehman I, Best SM, Bonfield W. Characterization of the transformation from calcium-deficient apatite to beta-tricalcium phosphate. J Mater Sci Mater Med 2000;11:533–539
18. Genge RB, Sauer RG, Wu YLN, McLean MF, Wuthier ER. Correlation between loss of alkaline phosphatase activity and accumulation of calcium during matrix vesicle-mediated mineralization. J Biol Chem 1988;263:18513–18519
19. Sowa H, Kaji H, Yamaguchi T, Sugimoto T, Chihara K. Smad3 promotes alkaline phosphatase activity and mineralization of osteoblastic MC3T-E1 cells. J Bone Miner Res 2002;17: 1190–1199
20. Wennberg C, Hessle L, Lundberg P, Mauro S, Narisawa S, Lerner HU, Millan LJ. Functional characterization of osteoblasts and osteoclasts from alkaline phosphatase knockout mice. J Bone Miner Res 2000;15:1879–1888
21. Anderson CH. Molecular biology of matrix vesicles. Clin Orthop 1995;314:266–280

Available online at www.sciencedirect.com
ScienceDirect
Biochemical and Biophysical Research Communications 359 (2007) 108–114
BBRC
www.elsevier.com/locate/ybbrc

FGF-2 suppresses cellular senescence of human mesenchymal stem cells by down-regulation of TGF-β2

Tomomi Ito [a,b], Rumi Sawada [a], Yoko Fujiwara [b], Yousuke Seyama [b], Toshie Tsuchiya [a,*]

[a] *Division of Medical Devices, National Institute of Health Sciences, 1-18-1 Kamiyoga, Setagaya-ku, Tokyo 158-8501, Japan*
[b] *Graduate School of Humanities and Sciences, Ochanomizu University, 2-1-1 Otsuka, Bunkyo-ku, Tokyo 112-8610, Japan*

Received 9 May 2007
Available online 21 May 2007

Abstract

Human mesenchymal stem cells (hMSCs) are able to both self-replicate and differentiate into a variety of cell types. Fibroblast growth factor-2 (FGF-2) stimulates the growth of hMSCs *in vitro*, but its mechanisms have not been clarified yet. In this study, we investigated whether cellular senescence was involved in the stimulation of hMSCs growth by FGF-2 and the expression levels of transforming growth factor-β1 and -β2 (TGF-βs). Because hMSCs were induced cellular senescence due to long-term culture, FGF-2 decreased the percentage of senescent cells and suppressed G1 cell growth arrest through the suppression of $p21^{Cip1}$, p53, and $p16^{INK4a}$ mRNA expression levels. Furthermore, the levels of TGF-βs mRNA expression in hMSCs were increased by long-term culture, but FGF-2 suppressed the increase of TGF-β2 mRNA expression due to long-term culture. These results suggest that FGF-2 suppresses the hMSCs cellular senescence dependent on the length of culture through down-regulation of TGF-β2 expression.

Keywords: Human mesenchymal stem cells; FGF-2; TGF-β; Cellular senescence; Cyclin-dependent kinase inhibitors; RB

Mesenchymal stem cells (MSCs) are able to self-replicate and differentiate into a variety of cell types such as osteoblasts, chondrocytes, adipocytes, and smooth muscle cells [1–5]. These capacities of MSCs have been used in studies of bone and cartilage regeneration [6–8]. One of the sources for human MSCs (hMSCs) is adult bone marrow. However, the ratio of hMSCs in adult bone marrow is about one per one-hundred-thousand nucleated cells [6], and the volume of bone marrow obtainable is limited. To secure the numbers of hMSCs required for the regeneration of tissues, hMSCs obtained from bone marrow need to be expanded *in vitro*.

Fibroblast growth factor-2 (FGF-2) is a cell growth factor involved in angiogenesis and tissue repair. FGF-2 maintains human bone marrow stromal cells in an immature state during *in vitro* expansion [9–11]. In hMSCs, FGF-2 enhances growth and maintains the potential for multidifferentiation [12,13]. Thus, it is thought that FGF-2 is one of the effective factors in the regeneration of tissues.

Transforming growth factor-βs (TGF-βs) are multifunctional proteins that regulate cell growth, differentiation, migration, extracellular matrix production, angiogenesis, and immunosuppression [14]. TGF-βs arrest the cell growth of epithelial cells and blood cells in the G1 phase through inhibition of G1 cyclin-dependent kinases (CDKs) [15,16]. It is reported that TGF-βs down-regulate the c-myc oncogene and up-regulate the CDK inhibitors $p15^{INK4b}$ and $p21^{Cip1}$ [17,18].

Cellular senescence is one of the tumor suppressor functions of normal human cells [19]. Senescent cells induce cell growth arrest in the G1 phase and a change in morphology and metabolism. Some of the senescence-associated changes that are common to many different cell types include cellular enlargement, increased lysosome biogenesis, and expression of a β-galactosidase that has a pH optimum of 6 (senescence-associated β-galactosidase or

* Corresponding author. Fax: +81 3 3700 9196.
E-mail address: tsuchiya@nihs.go.jp (T. Tsuchiya).

0006-291X/$ - see front matter © 2007 Elsevier Inc. All rights reserved.
doi:10.1016/j.bbrc.2007.05.067

SA-β-Gal) [20]. It is thought that two mechanisms of cellular senescence exist: intrinsic senescence dependent on telomere shortening and extrinsic senescence independent of it. The former is induced by activation of p53 and an increase of expression levels of $p21^{Cip1}$, a well-recognized p53 target gene [19,21–23]. The latter is induced by various culture stresses and the up-regulation of $p16^{INK4a}$ expression [24–26]. Activation of cyclin-CDK complex by suppression of expression of the CDK inhibitors $p21^{Cip1}$, p53, $p16^{INK4a}$ promotes phosphorylation of retinoblastoma proteins (pRB). Phosphorylation of pRB is required for the progress from the cellular G1 phase to the S phase.

Our previous studies have shown that hMSCs growth was decreased and the level of TGF-β mRNA expression increased during long-term subculture *in vitro* [27]. In this study, we investigated whether the decrease of growth ability in long-term culture involves cellular senescence through changes in the expressions of TGF-β and the CDK inhibitors. Moreover, we attempted to stimulate hMSCs growth using FGF-2 and investigated whether FGF-2 affected cellular senescence and the expressions of TGF-βs, cell growth suppression factors.

Materials and methods

Cell culture. hMSCs were obtained from Cambrex Bio Science Walkersville, Inc. (Walkersville, MD) and seeded in MSCGM medium (Cambrex Bio Science Walkersville) at 5000 cells/cm^2 with or without 1 ng/ml FGF-2 (BD Biosciences, Bedford, MA). FGF-2 was also added when the culture medium was changed every 2–3 days. The concentration of FGF-2 used in this study was based on a previous report [13]. The cells were maintained in humidified incubators at 37 °C with 5% CO_2.

TGF-β treatment. TGF-β1 and TGF-β2 (human, recombinant) were purchased from Sigma (St. Louis, MO). TGF-β1 or TGF-β2 at 5 ng/ml was added to the culture medium without FGF-2 for 5 days. The concentration of TGF-βs used was determined by a previously published study [28].

SA-β-Gal staining. SA-β-Gal staining was performed using a Senescence-associated β-Galactosidase Staining Kit (Cell Signaling, Beverly, MA) following the manufacturer's protocol.

BrdU incorporation. The incorporation of BrdU during DNA synthesis was measured using a Cell Proliferation ELISA kit with BrdU (Roche Diagnostics, Penzberg, Germany) following the manufacturer's protocol.

Flow cytometry analysis. hMSCs were removed from the culture dish with trypsin/EDTA (Cambrex Bio Science Walkersville), then stained using a CycleTEST™ PLUS DNA Reagent Kit (BD Biosciences, San Jose, CA) following the manufacturer's protocol. Propidium iodide (PI) fluorescence was measured using a FACSCalibur flow cytometer (BD Biosciences). The data were analyzed using FlowJo (Tree Star, Inc., Ashland, OR).

Quantitative real-time RT-PCR. PCRs of p53, TGF-β1, and TGF-β2 were performed for 35 cycles under the following conditions: denaturation at 95 °C for 10 s, annealing at 68 °C for 10 s, and extension at 72 °C for 16 s; of p16: 95 °C for 10 s, 60 °C for 10 s, 72 °C for 6 s; and p21: 95 °C for 10 s, 60 °C for 10 s, 72 °C for 10 s, using the LightCycler real-time PCR System (Roche Diagnostics, Tokyo, Japan). The primers for p53, TGF-β1, TGF-β2, and GAPDH were from a LightCycler-Primer Set (Search LC GmbH, Heidelberg, Germany). The primers for p16 and p21 were 5′-CACTCACGCCCTAAGC-3′ and 5′-GCAGTGTGACTCAAGAGAA-3′, and 5′-TTGATTAGCAGCGGAACA-3′ and 5′-GGAGAAACGG GAACCAG-3′, respectively.

Western blotting. A mouse monoclonal antibody against pRb and a rabbit polyclonal antibody against phospho-pRb were purchased from Cell Signaling (Beverly, MA). The rabbit polyclonal antibodies against TGF-β1, TGF-β2, and GAPDH were purchased from Santa Cruz Biotechnology, Inc. The bands were quantified using ImageQuant™ TL (GE Healthcare UK Ltd., Buckingham, England).

Results

TGF-β induced cellular senescence in hMSCs

To investigate the effects of TGF-β on cellular senescence, hMSCs were cultured in MSCGM medium supplemented with TGF-β1 or TGF-β2, and then SA-β-Gal staining was performed and incorporation of BrdU, an analog of thymidine, was measured. One day after TGF-β1 or TGF-β2 treatment, hMSCs had a fibroblast-like morphology (Fig. 1C and E) similar to the control (Fig. 1A). Five days after TGF-β1 or TGF-β2 treatment, hMSCs had acquired a depressed morphology, and some of them were stained blue by SA-β-Gal staining (Fig. 1D and F, arrows). In the control, however, stained cells were rarely observed (Fig. 1B). Five days after TGF-β1 and TGF-β2 treatment, BrdU incorporation had decreased in comparison with the control (Fig. 1G). Furthermore, to confirm whether TGF-βs induced G1 cell growth arrest in hMSCs, cell cycle analysis was performed using flow cytometry. As shown in Fig. 1H, TGF-β1 and TGF-β2 increased the percentage of cells in G1 phase, and decreased it in S and G2 phases. Then, the mRNA expression levels of $p16^{INK4a}$, $p21^{Cip1}$, and p53, CDK inhibitors of the G1 phase, and the protein expression levels of pRB were measured after 5 days of TGF-β1 or TGF-β2 treatment. TGF-βs increased all three mRNA expression levels (Fig. 1I–K). On the other hand, the phosphorylated pRB (ppRB) expression was decreased by both TGF-βs (Fig. 1L). These results suggest that cellular senescence of hMSCs is induced through G1 growth arrest by TGF-β1 and TGF-β2.

FGF-2 suppressed hMSCs cellular senescence

To investigate whether stimulation of hMSCs growth by FGF-2 was involved in the suppression of cellular senescence, hMSCs were stained with SA-β-Gal after culture with or without FGF-2 (FGF-2(+) or FGF-2(−)) for 10 or 50 days. After 10 days' culture in FGF-2(−), hMSCs had a fibroblast-like morphology, and 20.5% of the cells were stained blue by SA-β-Gal (Fig. 2A); however, after 50 days' culture, hMSCs had developed a depressed morphology, and 57.6% of the cells were stained blue (Fig. 2C, arrows). After 10 or 50 days' culture in FGF-2(+), hMSCs morphology had a fibroblast-like morphology; moreover, 35.8% or 27.3% of the cells were stained blue, respectively (Fig. 2B and D). BrdU incorporation into hMSCs after 50 days' culture was 40% lower than after 10 days' culture in FGF-2(−) but not in FGF-2(+) (Fig. 2E). Furthermore, we investigated the effects of FGF-2 on the cell cycle. After 50 days' culture in FGF-2(−), the number of cells in the G1 phase was increased, but not after culture in FGF-2(+) (Fig. 2F).

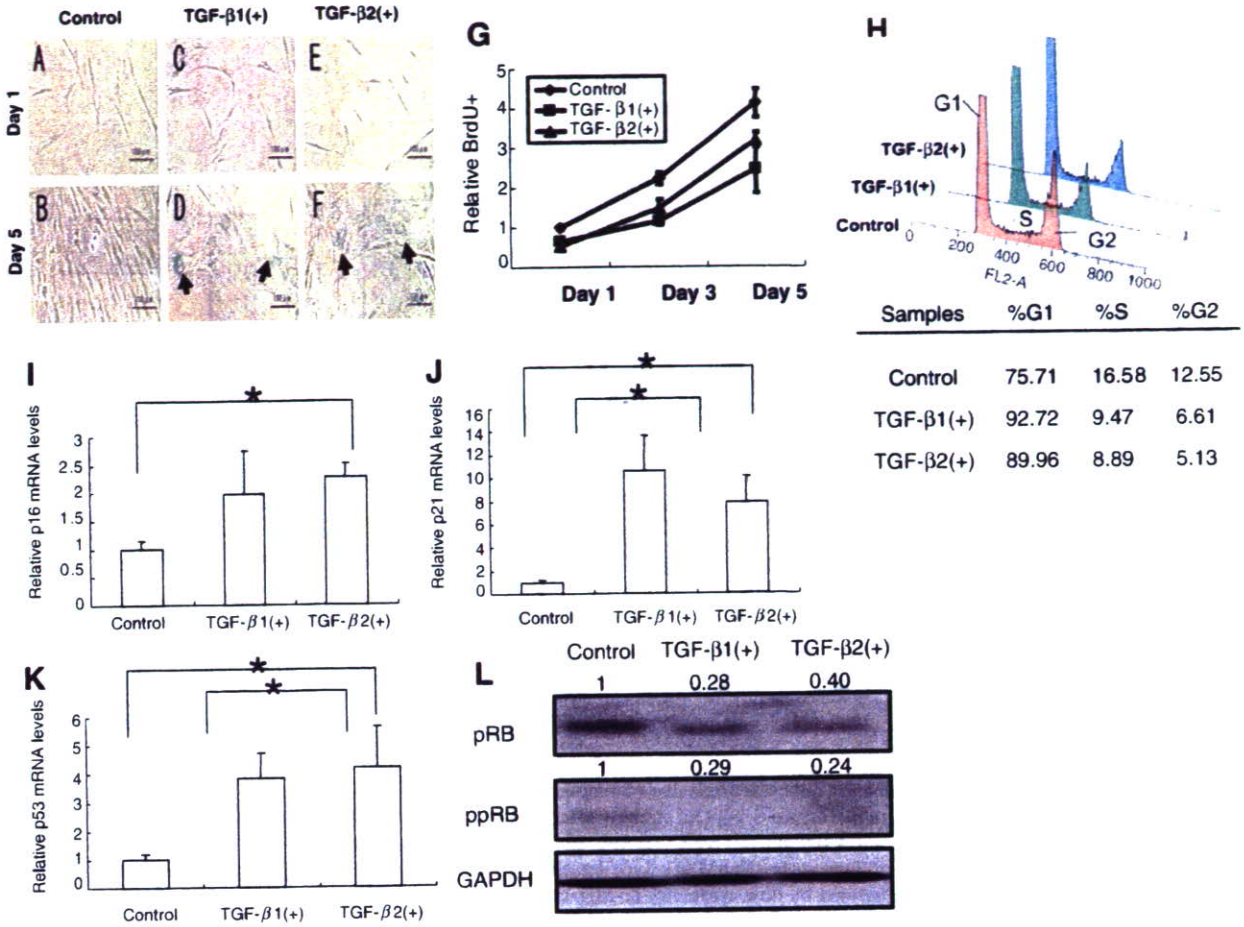

Fig. 1. TGF-β1 and β2 induce cellular senescence through G1 cell cycle arrest in hMSCs. hMSCs were maintained as an untreated control or treated with 5 ng/ml TGF-β1 or TGF-β2 for 5 days. (A–F) hMSCs were performed SA-β-Gal staining 1 or 5 days after TGF-β treatment (Day 1 or 5). The arrows in (D) and (F) indicate the senescent cells stained blue. The scale bar is 100 μm. (G) BrdU incorporation into hMSCs was assayed at Days 1, 3, and 5. Each point represents quantities relative to the untreated control at Day 1. (H) After 3 days' culture with or without TGF-β1 or TGF-β2, cells were removed from the culture dish with trypsin/EDTA, fixed, stained for DNA with PI, and analyzed by flow cytometry (*y*-axis, cell count; *x*-axis, PI intensity). (I–K) $p16^{INK4a}$ (A), p53 (B), and $p21^{Cip1}$ (C) mRNA expression levels measured using real time RT-PCR. The relative levels of gene expression of target mRNA were normalized to GAPDH expression. Values are means ± SD of three experiments ($^*P < 0.05$). (L) total pRB and phospho-pRB proteins detected using Western blot analysis.

The mRNA expression levels of $p16^{INK4a}$, $p21^{Cip1}$, and p53 and the expression levels of pRB in hMSCs were measured after culture for 10 or 50 days in FGF-2(−) or FGF-2(+). After 50 days' culture in FGF-2(−), the mRNA expression levels of $p16^{INK4a}$, $p21^{Cip1}$, and p53 were significantly higher than after 10 days' culture, but not after culture in FGF-2(+) (Fig. 3A–C). On the other hand, after 50 days' culture in FGF-2(−), the expression levels of total pRB and ppRB were decreased compared with after 10 days' culture, but not after culture in FGF-2(+) (Fig. 3D). These results suggest that FGF-2 suppresses hMSCs cellular senescence depending on the length of culture.

FGF-2 influenced TGF-β mRNA expression in hMSCs

To investigate the effects of FGF-2 on TGF-β mRNA and protein expression levels in hMSCs, their levels were measured after culture for 1, 10, or 50 days in FGF-2(−) or FGF-2(+). After culture for 50 days in both FGF-2(−) and FGF-2(+), TGF-β1 mRNA expression levels of hMSCs had increased in comparison with culture for 1 and 10 days (Fig. 4A). On the other hand, TGF-β2 mRNA expression levels were higher after 50 days' culture in FGF-2(−) than after 10 days, but not after culture in FGF-2(+) (Fig. 4B). Comparing 50 days' culture with 10 days' culture, the changes of TGF-β1 and TGF-β2 protein expression levels paralleled the results of mRNA expression levels (Fig. 4C). These results suggest that FGF-2 has no effect on TGF-β1 expression levels in hMSCs, but inhibits the increase of TGF-β2 expression, depending on the length of culture.

Discussion

hMSCs are one of the human tissue stem cells, and they maintain the homeostasis of bone and cartilage. hMSCs

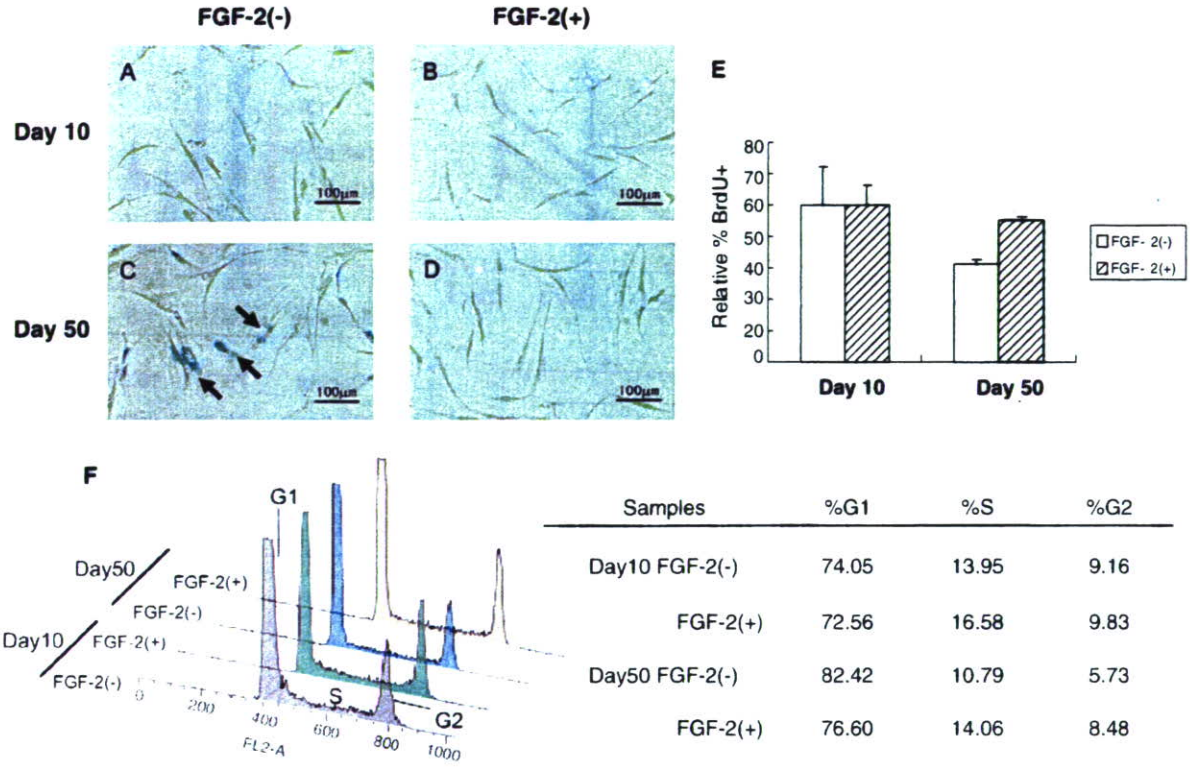

Samples	%G1	%S	%G2
Day10 FGF-2(-)	74.05	13.95	9.16
FGF-2(+)	72.56	16.58	9.83
Day50 FGF-2(-)	82.42	10.79	5.73
FGF-2(+)	76.60	14.06	8.48

Fig. 2. FGF-2 suppresses cellular senescence through G1 cell cycle arrest due to long-term culture. hMSCs were maintained in the medium in the presence or absence of FGF-2 (1 ng/ml). (A–D) hMSCs were performed SA-β-Gal staining after culture for 10 days or 50 days (Day 10 or 50). The arrows in (C) indicate senescent cells that stained blue. The scale bar is 100 μm. (E) BrdU incorporation into hMSCs was assayed at Days 10 and 50. Each bar represents quantities relative to Day 10 and is average ± SD of three wells. (F) hMSCs were detached from the culture dish with trypsin/EDTA after culture at Days 10 and 50, fixed, stained for DNA with PI, and analyzed by flow cytometry (*y*-axis, cell count; *x*-axis, PI intensity).

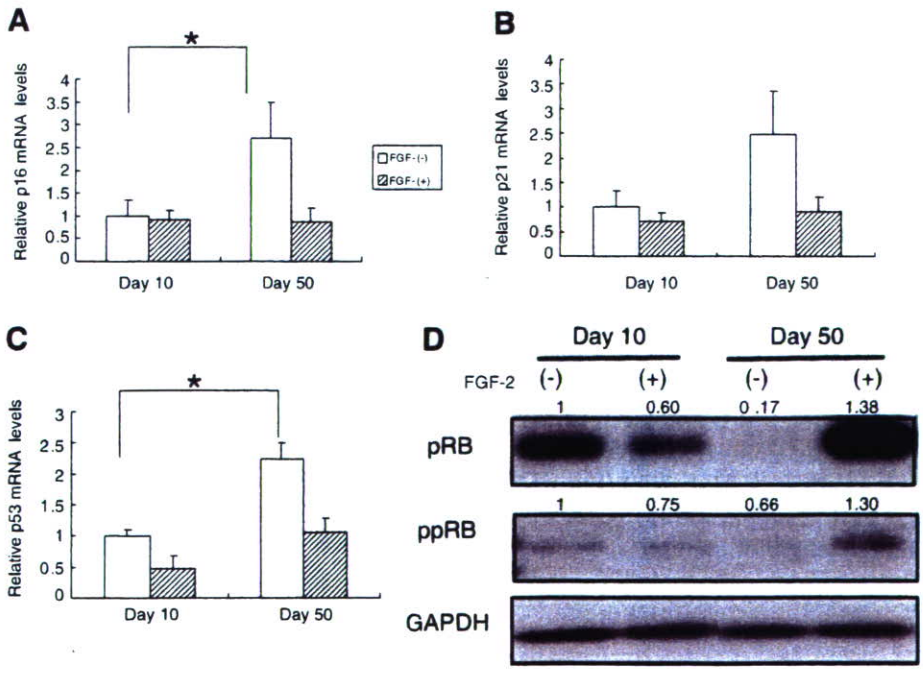

Fig. 3. FGF-2 suppresses G1 cell cycle arrest due to passaging. hMSCs were maintained in the medium in the presence or absence of FGF-2 (1 ng/ml), and total RNAs and proteins were extracted when approaching confluence. (A–C) $p16^{INK4a}$ (A), p53 (B), and $p21^{Cip1}$ (C) mRNA expression levels were measured using real time RT-PCR at Days 10 and 50. (D) Total pRB and phospho-pRB proteins detected using Western blot analysis at Days 10 and 50.

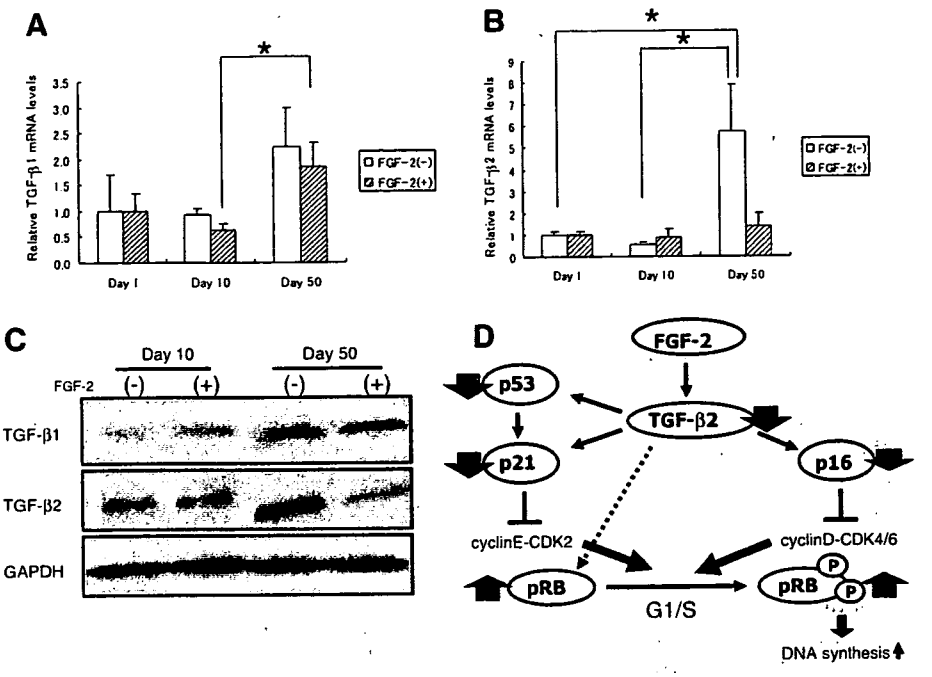

Fig. 4. FGF-2 increases TGF-β1 mRNA expression levels, but does not increase TGF-β2 during long-term culture. hMSCs were maintained in the medium in the presence or absence of FGF-2 (1 ng/ml), and total RNAs and proteins were extracted when the cells approached confluence. (A,B) TGF-β1 and β2 mRNA expression levels were measured using real time RT-PCR at Days 1, 10, and 50. (C) TGF-β1 and β2 protein expression levels were detected using Western blot analysis at Days 10 and 50.

are found in adult human bone marrow, and those obtained from patients until late adulthood still exhibit osteogenic potency [29]. Thus, it is thought that hMSCs maintain self-renewal and differentiation capacity *in vivo* throughout life. However, our previous studies have shown that the self-renewal potency of hMSCs is decreased by long-term culture *in vitro* [27]. The results of this study suggest that cellular senescence was induced in hMSCs (Fig. 2) following G1 cell growth arrest through increases of $p16^{INK4a}$, $p21^{Cip1}$, and p53 mRNA expression levels (Figs. 2 and 3) due to long-term culture *in vitro*. Since it was reported that cellular senescence was induced by the stress of culture [30], hMSCs would also be subject to finite proliferation due to many unknown stresses in our studies.

It was reported that TGF-β1 induced changes in hMSC morphology [28]. In the present study, after 5 days' treatment with TGF-β1 and TGF-β2 (TGF-βs), hMSCs were spread out, some of the cells were stained blue by SA-β-Gal staining (Fig. 1A–F), and they had decreased DNA replicative potential (Fig. 1G). In human prostate stromal cells, TGF-β1 induced similar morphological changes, but had no effect on cellular senescence [31]. However, we hypothesize that the changes in hMSC morphology induced by TGF-βs were due to cellular senescence because the conditions of our study differed from those of previous studies: hMSCs were treated with 5 ng/ml TGF-βs for 5 days in this study (Fig. 1), whereas hMSCs were treated with 1 ng/ml TGF-β1 for 3 days in the previous study [31]. Moreover, the responses to TGF-β stimulation may depend on the kind of cell.

We considered that the cellular senescence induced by TGF-βs is involved in G1 growth arrest through the increase of CDK inhibitors ($p16^{INK4a}$, $p21^{Cip1}$, and p53). We observed that the number of cells in the G1 phase (Fig. 1) and the mRNA expression levels of $p16^{INK4a}$, $p21^{Cip1}$, and p53 were increased by TGF-βs (Fig. 2A–C). It has been reported that TGF-β increased the expression levels of $p21^{Cip1}$ [17] but not $p16^{INK4a}$ [18,32]. However, the increase of $p16^{INK4a}$ expression levels was important for the irreversible stop of the cell cycle [26]. Based on our results in this study, we support the latter report.

The phosphorylation of pRB, which is regulated by CDK inhibitors, accompanies the G1/S transition [16,33]. We also showed that the expression levels of total pRB and ppRB were decreased by TGF-βs treatment (Fig. 2D). It has been reported that TGF-β1 decreased RB gene expression [34] moreover, TGF-β1 inhibited pRB phosphorylation [15,35]. We suspect that ppRB expression decreased for two reasons: the relative decrease due to the inhibition of total pRB expression by TGF-βs and the decrease of pRB phosphorylation due to the increase of CDK inhibitors by TGF-βs.

FGF-2, one of the cell growth factors, efficiently increases the number of hMSCs [12,13], but its mechanisms have unknown yet. In this study, we showed that the cell growth arrest in the G1 phase was suppressed by FGF-2 through the suppression of $p16^{INK4a}$, $p21^{Cip1}$, and p53 mRNA expression levels and the increase of ppRB expression levels (Figs. 2 and 3). Furthermore, the expression levels of TGF-β1 and β2 mRNA were increased by long-term

culture (Fig. 4A and B), in agreement with our previous studies [27]. However, FGF-2 suppressed the increase of TGF-β2 mRNA expression levels (Fig. 4B). FGF-2 also consistently suppressed the increase of TGF-β2 protein expression levels in long-term culture (Fig. 4C). It was reported that TGF-β2 inhibited FGF-2-induced proliferation of corneal endothelial cells [36]. Based on our results and that report, we consider that FGF-2 suppressed cellular senescence through down-regulation of TGF-β2 expression in hMSCs (Fig. 4D).

After 50 days' culture with FGF-2, pRB protein expression levels were remarkably increased, ppRB expression levels were up-regulated (Fig. 3D), and TGF-β2 expression was down-regulated as well (Fig. 4B). Moreover, TGF-βs remarkably decreased the pRB expression levels and induced cellular senescence (Fig. 1). It was also reported that senescence in cells induced reduction of RB protein levels [37]. Therefore, the increase of pRB expression levels when FGF-2 suppressed hMSC senescence may be involved in the down-regulation of TGF-β2 (Fig. 4D).

In conclusion, long-term culture induced cellular senescence by arresting cell growth in the G1 phase and increasing expression levels of TGF-βs in hMSCs. On the other hand, FGF-2 suppressed cellular senescence and down-regulated TGF-β2 expression in hMSCs. We consider that the suppression of TGF-β2 expression is important in the suppression of cellular senescence of hMSCs by FGF-2. However, after 150 days' culture, hMSCs no longer maintained self-renewal capacity, and the expression levels of TGF-β2 were increased in spite of the addition of FGF-2 (data not shown). These results suggest that FGF-2 delayed the decrease of self-renewal capacity due to long-term culture in hMSCs. TGF-β2 may be useful for the maintenance of self-renewal capacity in hMSCs. The data in this study will advance the knowledge of hMSC biology, and allow us to realize safe and efficient clinical applications of hMSCs.

References

[1] M.F. Pittenger, A.M. Mackay, S.C. Beck, R.K. Jaiswal, R. Douglas, J.D. Mosca, M.A. Moorman, D.W. Simonetti, S. Craig, D.R. Marshak, Multilineage potential of adult human mesenchymal stem cells, Science 284 (1999) 143–147.

[2] A.I. Caplan, S.P. Bruder, Mesenchymal stem cells: building blocks for molecular medicine in the 21st century, Trends Mol. Med. 7 (2001) 259–264.

[3] S. Gojo, N. Gojo, Y. Takeda, T. Mori, H. Abe, S. Kyo, J. Hata, A. Umezawa, In vivo cardiovasculogenesis by direct injection of isolated adult mesenchymal stem cells, Exp. Cell Res. 288 (2003) 51–59.

[4] S. Wakitani, T. Saito, A.I. Caplan, Myogenic cells derived from rat bone marrow mesenchymal stem cells exposed to 5-azacytidine, Muscle Nerve 18 (1995) 1417–1426.

[5] J.P. Darwin, Marrow stromal cells as stem cells for nonhematopoietic tissues, Science 276 (1997) 71–74.

[6] H. Ohgushi, A.I. Caplan, Stem cell technology and bioceramics: from cell to gene engineering, J. Biomed. Mater. Res. 48 (1999) 913–927.

[7] H. Petite, V. Viateau, W. Bensaid, A. Meunier, C. Pollak, M. Bourguignon, K. Oudina, L. Sedel, G. Guillemin, Tissue-engineered bone regeneration, Nat. Biotechnol. 18 (2000) 959–963.

[8] M. Ochi, N. Adachi, N. Hiroo, S. Yamada, Y. Ito, M. Agung, Articular cartilage repair using tissue engineering technique-novel approach with minimally invasive procedure, Artif. Organs 28 (2004) 28–32.

[9] M. Mastrogiacomo, R. Cancedda, R. Quarto, Effect of different growth factors on the chondrogenic potential of human bone marrow stromal cells, Osteoarthritis Cartilage 9 (Suppl. A) (2001) S36–S40.

[10] I. Martin, A. Muraglia, G. Campanile, R. Cancedda, R. Quarto, Fibroblast growth factor-2 supports ex vivo expansion and maintenance of osteogenic precursors from human bone marrow, Endocrinology 138 (1997) 4456–4462.

[11] G. Bianchi, A. Banfi, M. Mastrogiacomo, R. Notaro, L. Luzzatto, R. Cancedda, R. Quarto, Ex vivo enrichment of mesenchymal stem cell progenitors by fibroblast growth factor 2, Exp. Cell Res. 287 (2003) 98–105.

[12] L.A. Solchaga, K. Penick, J.D. Porter, V.M. Goldberg, A.I. Caplan, J.F. Welter, FGF-2 enhances the mitotic and chondrogenic potentials of human adult bone marrow-derived mesenchymal stem cells, J. Cell Physiol. 203 (2005) 398–409.

[13] S. Tsutsumi, A. Shimazu, K. Miyazaki, H. Pan, C. Koike, E. Yoshida, K. Takagishi, Y. Kato, Retention of multilineage differentiation potential of mesenchymal stem cells during proliferation in response to FGF, Biochem. Biopys. Res. Commun. 288 (2001) 413–419.

[14] K. Miyazono, H. Suzuki, T. Imamura, Regulation of TGF-β signaling and its roles in progression of tumors, Cancer Sci. 94 (2003) 230–234.

[15] M. Laiho, J.A. DeCaprio, J.W. Ludlow, D.M. Livingston, J. Massague, Growth inhibition by TGF-β linked to suppression of retinoblastoma protein phosphorylation, Cell 62 (1990) 175–185.

[16] J. Charles, M.R. Jeames, CDK inhibitors: positive and negative regulators of G1-phase progression, Genes & Development 13 (1999) 1501–1512.

[17] J. Massague, S.W. Blain, R.S. Lo, TGF-β signaling in growth control, cancer, and heritable disorders, Cell 103 (2000) 295–309.

[18] W. Zhou, I. Park, M. Pins, J.M. Kozlowski, B. Jovanovic, J. Zhang, C. Lee, K. Ilio, Dual regulation of proliferation and growth arrest in prostatic stromal cells by transforming growth factor-β1, Endocrinology 144 (2003) 4280–4284.

[19] K. Itahana, G. Dimri, J. Campisi, Regulation of cellular senescence by p53, Eur. J. Biochem. 268 (2001) 2784–2791.

[20] G.P. Dimri, X. Lee, G. Basile, G. Scott, C. Roskelley, E.E. Medrano, M. Linskens, I. Rubelj, O. Pereira-Smith, M. Peacocke, J. Campisi, A biomarker that identifies senescent human cells in culture and in aging skin in vivo, Proc. Natl. Acad. Sci. USA 92 (1995) 9363–9367.

[21] W.S. el-Deiry, T. Tokino, V.E. Velculescu, D.B. Levy, R. Parsons, J.M. Trent, D. Lin, W.E. Mercer, K.W. Kinzler, B. Vogelstein, WAF1, a potential mediator of p53 tumor suppression, Cell 75 (1993) 817–825.

[22] J. LaBaer, M.D. Garrett, L.F. Stevenson, J.M. Slingerland, C. Sandhu, H.S. Chou, A. Fattaey, E. Harlow, New function activities for the p21 family of CDK inhibitors, Genes. Dev. 11 (1997) 847–862.

[23] K. Itahana, G.P. Dimri, E. Hara, Y. Itahana, Y. Zou, P.Y. Desprez, J. Campisi, A role for p53 in maintaining and establishing the quiescence growth arrest in human cells, J. Biol. Chem. 277 (2002) 18206–18214.

[24] T. Kiyono, S.A. Foster, J.I. Koop, J.K. McDougall, D.A. Galloway, A.J. Klingelhutz, Both Rb/p16^{INK4a} inactivation and telomerase activity are required to immortalize human epithelial cells, Nature 396 (1998) 84–88.

[25] J.G. Rheinwald, W.C. Hahn, M.R. Ramsey, J.Y. Wu, Z. Guo, H. Tsao, M. Luca, C. Catricala, K.M. O'Toole, A two-stage, p16 (INK4A)- and p53-dependent keratinocyte senescence mechanism that limits replicative potential independent of telomere status, Mol. Cell Biol. 22 (2002) 5157–5172.

[26] C.M. Beausejour, A. Krtolica, F. Galimi, M. Narita, S.W. Lowe, P. Yaswen, J. Campisi, Reversal of human cellular senescence: roles of the p53 and p16 pathways, EMBO J. 22 (2003) 4212–4222.